Inorganic Chemistry

Article

pubs.acs.org/IC

Assessing the Impact of Electronic and Steric Tuning of the Ligand in the Spin State and Catalytic Oxidation Ability of the Fe^{II}(Pytacn) Family of Complexes

Irene Prat,[†] Anna Company,*[,†] Teresa Corona,[†] Teodor Parella,[‡] Xavi Ribas,[†] and Miquel Costas*[,†]

[†]Grup de Química Bioinorgànica i Supramolecular (QBIS), Institut de Química Computacional i Catàlisi (IQCC) and Departament de Química, Universitat de Girona, Campus Montilivi, E17071 Girona, Catalonia, Spain

[‡]Servei de Ressonància Magnètica Nuclear, Universitat Autònoma de Barcelona, Bellaterra, E08193 Barcelona, Catalonia, Spain

Supporting Information

ABSTRACT: A family of iron complexes with the general formula $[Fe^{II}(^{R,R'}Pytacn)(X)_2]^{n+}$ is described, where $^{R,R'}$Pytacn is the tetradentate ligand 1-[(4-R′-6-R-2-pyridyl)methyl]-4,7-dimethyl-1,4,7-triazacyclononane, R refers to the group at the α-position of the pyridine, R′ corresponds to the group at the γ-position, and X denotes CH_3CN or CF_3SO_3. Herein, we study the influence of the pyridine substituents R and R′ on the electronic properties of the coordinated iron center by a combination of structural and spectroscopic characterization using X-ray diffraction, ^{1}H NMR and UV−vis spectroscopies, and magnetic susceptibility measurements. The electronic properties of the substituent in the γ-position of the pyridine ring (R′) modulate the strength of the ligand field, as shown by magnetic susceptibility measurements in CD_3CN solution, which provide a direct indication of the population of the magnetically active high-spin S = 2 ferrous state. Indeed, a series of complexes $[Fe^{II}(^{H,R'}Pytacn)(CD_3CN)_2]^{2+}$ exist as mixtures of high-spin (S = 2) and low-spin (S = 0) complexes, and their effective magnetic moment directly correlates with the electron-releasing ability of R′. On the other hand, the substitution of the hydrogen atom in the α-position of the pyridine by a methyl, chlorine, or fluorine group favors the high-spin state. The whole family of complexes has been assayed in catalytic C−H and C═C oxidation reactions with H_2O_2. These catalysts exhibit excellent efficiency in the stereospecific hydroxylation of alkanes and in the oxidation of olefins. Remarkably, R′-substituents have little influence on the efficiency and chemoselectivity of the catalytic activity of the complexes, but the selectivity toward olefin *cis*-dihydroxylation is enhanced for complexes with R = Me, F, or Cl. Isotopic labeling studies in the epoxidation and *cis*-dihydroxylation reactions show that R has a definitive role in dictating the origin of the oxygen atom that is transferred in the epoxidation reaction.

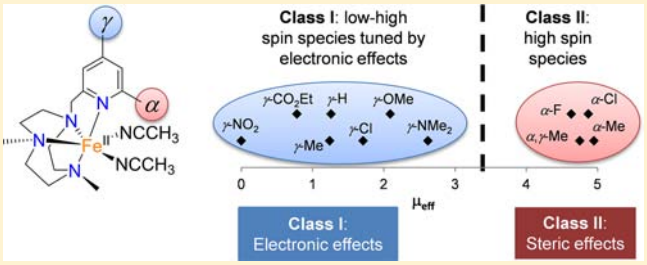

INTRODUCTION

There is a growing interest in the development of transition-metal complexes that can catalyze the selective oxidation of C−H and C═C bonds using green oxidants such as O_2 or peroxides with novel and better selectivities and efficiencies than traditional less-sustainable methodologies.[1] In this regard, iron is a particularly attractive metal for catalyst development because of its high availability and lack of toxicity.[2] Because several highly selective oxygenases contain iron in their active site,[3,4] nature constitutes a source of inspiration for the design of such iron oxidation catalysts.[5] For example, Rieske oxygenases are enzymes that bear a mononuclear nonheme iron center in their active center, and they use O_2 to catalyze the hydroxylation of alkyl aromatic moieties and the *cis*-dihydroxylation of arenes in the first step of the degradation of persistent pollutants.[6]

Taking into consideration the ability of mononuclear iron sites to mediate oxidation reactions in a selective manner, several families of bioinspired mononuclear nonheme iron complexes have been developed and tested during the past decade in the challenging oxidation of C−H and C═C bonds.[7−9] Selected families are capable of eliciting enzyme-like reactivity, meaning that they can mediate oxidations through metal-centered processes without a significant involvement of free diffusing radicals.[5a,b] Such studies have shown that the activity of these complexes as oxidation catalysts depends, in a very delicate manner, on a number of aspects. Some of them are rather obvious such as metal nuclearity, ligand denticity, strength of metal binding, presence of available coordination sites, nature of the ligand donor set, or the oxidatively robust nature of the ligand. However, other subtler aspects have been identified, which include ligand field and coordination topology.[10] Presumably, interconnections among multiple aspects exist, and this complexity makes structure−activity correlations challenging.

Received: February 15, 2013
Published: July 31, 2013

   dx.doi.org/10.1021/ic4004033 | *Inorg. Chem.* 2013, 52, 9229−9244

Scheme 1. Ligands and Complexes Employed in This Work

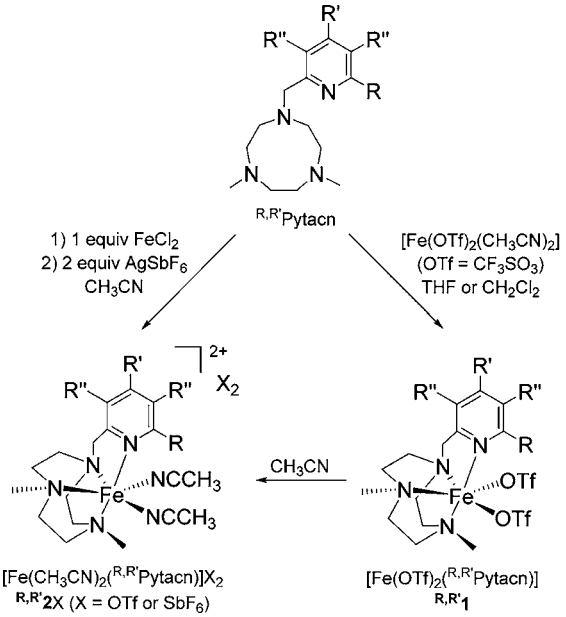

ligand	R	R'	R''
^{H,H}Pytacn	H	H	H
^{H,NMe2}Pytacn	H	NMe_2	H
^{H,OMe}Pytacn	H	OMe	Me
^{H,Me}Pytacn	H	Me	H
^{H,Cl}Pytacn	H	Cl	H
^{H,CO2Et}Pytacn	H	CO_2Et	H
^{H,NO2}Pytacn	H	NO_2	H
^{Me,H}Pytacn	Me	H	H
^{Me,Me}Pytacn	Me	Me	H
^{Cl,H}Pytacn	Cl	H	H
^{F,H}Pytacn	F	H	H

Most iron complexes that carry out selective C−H and C═C oxidation reactions share some structural features that include: (i) exchangeable coordination sites that can engage in fast substitution reactions with the oxidant, and (ii) ligand sets that can support iron centers in high oxidation states. Because of that, electronic factors that influence the lability of the complexes and the redox properties of the iron centers might have a significant impact on the catalytic activity. Electronic properties of the iron center can be modulated not only by the electron-donating ability of the ligand but also by the strength of the ligand field, as this directly determines the spin state. Spin state determines the lability of the complexes because high-spin complexes are inherently faster than their low-spin analogues in substitution reactions.

We have previously reported a family of iron complexes containing tetradentate ligands composed of a 1,4,7-triazacyclononane arm derivatized with a methylpyridine arm. Complexes $[Fe(CF_3SO_3)_2(^{H,H}Pytacn)]$ (^{H,H}**1**) and $[Fe(CF_3SO_3)_2(^{Me,H}Pytacn)]$ (^{Me,H}**1**) (Scheme 1) exhibit efficient catalytic activity in the stereospecific hydroxylation of alkanes and the epoxidation and *cis*-dihydroxylation of alkenes using H_2O_2 as an oxidant.[11] As ascertained by several mechanistic probes, these oxidative transformations occur through the mediation of a high-valent iron−oxo species.[11,12] Moreover, compound ^{H,H}**1** is highly active in the oxidation of water to generate O_2 using cerium as the sacrificial oxidizing reagent in a process that mimics what occurs in photosystem II.[13]

In this work, the basic structure of ^{H,H}**1** has been modified by introducing a range of substituents in the α- and γ-positions of the pyridine ring with different electronic and steric properties. We aim at evaluating the influence of these substituents in the electronic structure, as well as in the spectroscopic and structural features of the resulting iron(II) compounds, by means of several spectroscopic techniques both in the solid state and in solution. Herein, we show how the straightforward substitution of the pyridine ring of the primary Pytacn structure leads to important modifications in the electronic properties of the iron(II) center, which in some cases is translated into substantial changes in the spin-crossover properties of the metal site. In order to evaluate how the substitution in the pyridine ring affects the catalytic activity of the resulting iron complexes, we have studied their catalytic performance in the oxidation of cyclohexane and cyclooctene, which constitute model substrates for C−H hydroxylation and C═C oxidation reactions, respectively.

RESULTS AND DISCUSSION

Synthesis of Ligands and Complexes. A family of tetradentate ligands ($^{R,R'}$Pytacn, Scheme 1), which contains a functionalized triazacyclononane ring that has different methylpyridine derivatives with distinctive electronic and steric properties, has been prepared. These ligands constitute an extension of the previously described ^{H,H}Pytacn ligand, whose iron[11−13] and manganese[14] complexes were reported as robust and efficient oxidation catalysts. The introduction of several R′ groups with different electronic properties in the γ-position of the pyridine heterocycle (R′ = NMe_2, OMe, Me, H, Cl, CO_2Et, NO_2) is aimed at evaluating putative electronic effects without interference caused by steric effects. Instead, modification of the α-position of the pyridine ring (R = H, Me, F, Cl) not only affects the electronic properties but also enables tuning of the steric crowding around the iron metal site (Scheme 1).

$^{R,R'}$Pytacn ligands were prepared by alkylation of 1,4-dimethyl-1,4,7-triazacyclononane with the corresponding substituted picolyl chloride arm in acetonitrile and were obtained as pale yellow oils in good yields (67−73%).

Reaction of the tetradentate $^{R,R'}$Pytacn ligands with $[Fe(OTf)_2(CH_3CN)_2]$ (OTf = trifluoromethanesulfonate anion) in THF or CH_2Cl_2 under anaerobic conditions afforded the desired bis-triflato complexes, $[Fe(OTf)_2(^{R,R'}Pytacn)]$ ($^{R,R'}$**1**). Slow diffusion of diethyl ether over saturated CH_2Cl_2 solutions afforded $^{R,R'}$**1** as a crystalline material in 27−77% yields (Scheme 1). Following the synthetic procedure previously described for the preparation of $[Fe(CH_3CN)_2(^{H,H}Pytacn)](PF_6)_2$ (^{H,H}**2**PF_6),[11a] ^{H,H}**2**SbF_6 and ^{Me,H}**2**SbF_6 were synthesized in a one-pot reaction by mixing ^{H,H}Pytacn or ^{Me,H}Pytacn with 1 equiv of $FeCl_2$ in acetonitrile and with posterior addition of 2 equiv of $AgSbF_6$ in acetonitrile. Subsequent removal of the

dx.doi.org/10.1021/ic4004033 | Inorg. Chem. 2013, 52, 9229−9244

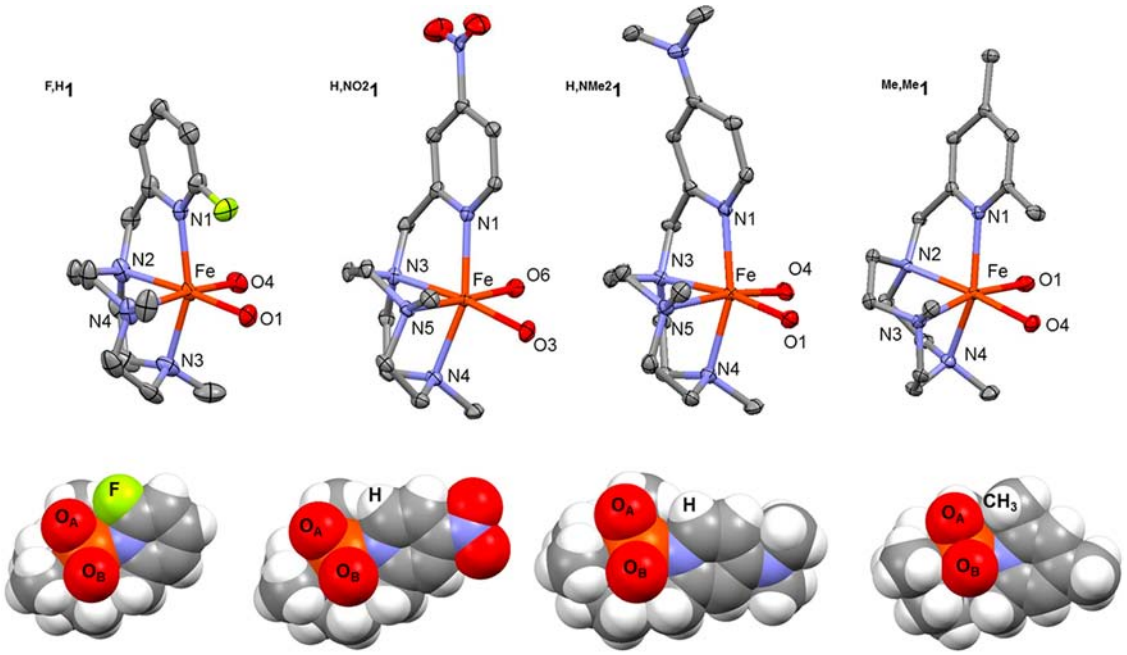

Figure 1. (Top) X-ray structures of ^{F,H}**1**, ^{H,NO2}**1**, ^{H,NMe2}**1**, and ^{Me,Me}**1**. Hydrogen atoms and triflate groups have been omitted for clarity except for the oxygen atoms directly bound to the iron center. (Bottom) Space-filling diagrams for complexes ^{F,H}**1**, ^{H,NO2}**1**, ^{H,NMe2}**1**, and ^{Me,Me}**1**. Triflate groups have been omitted for clarity, but the oxygen atoms directly bound to the iron center are represented.

precipitated AgCl and slow diethyl ether diffusion over the resulting solutions afforded the desired complexes as crystalline solids.

Solid-State Characterization. The solid-state molecular structure of complexes $^{R,R'}$**1** can be established by X-ray diffraction analysis. The crystal structures of ^{H,H}**1**, the diaquo complex $[Fe^{II}(H_2O)_2(^{Me,H}Pytacn)](OTf)_2$, and ^{H,H}**2**$PF_6$ have been previously reported,[11,12] while the structures of ^{H,NMe2}**1**, ^{H,OMe}**1**, ^{H,Me}**1**, ^{H,Cl}**1**, ^{H,CO2Et}**1**, ^{H,NO2}**1**, ^{Me,Me}**1**, ^{Cl,H}**1**, and ^{F,H}**1** are described for the first time in the present work. Compound ^{Me,H}**1** crystallizes as very thin needles not suitable for X-ray diffraction. Instead, the corresponding bis-acetonitrile complex ^{Me,H}**2**SbF_6 forms colorless rectangles, which can be measured by X-ray diffraction at different temperatures (100 and 300K), showing a spin transition in the solid state (vide infra).

As representative examples of the bis-triflato complexes, the X-ray structures of complexes ^{F,H}**1**, ^{H,NO2}**1**, ^{H,NMe2}**1**, and ^{Me,Me}**1** are depicted in Figure 1, experimental details of their crystal-structure determination are collected in Table 1, and a list of selected bond distances and angles can be found in Table 2. The same information for ^{Cl,H}**1**, ^{H,Me}**1**, ^{H,Cl}**1**, ^{H,CO2Et}**1**, and ^{H,OMe}**1** is found in the Supporting Information (Tables S1−S4 and Figures S1 and S2). These complexes crystallize in the monoclinic or orthorhombic crystal system, and they contain an iron(II) center in a distorted octahedral coordination geometry. Four coordination sites are occupied by the nitrogen atoms of the ligands, with the three N atoms of the triazacyclononane (tacn) macrocycle bound facially. That leaves two coordination sites in a relative *cis* configuration that are accessible for binding to triflate anions. The pyridine arm binds *trans* to one of the *N*-methyl groups of the ligand, and the other two nitrogen atoms of the tacn ligand are *trans* to the triflate ligands. Average Fe−N bond distances for these complexes are 2.1−2.2 Å, characteristic of high-spin Fe^{II} complexes.[15]

Despite the similarities in the structure for the whole range of bis-triflato complexes $^{R,R'}$**1**, some systematic differences arise when they are analyzed in more detail. The Fe−N_{py} bond length changes systematically depending on the substitution in the α-position of the pyridine ring; this value is 2.21 in ^{Me,Me}**1**, 2.26 in ^{Cl,H}**1**, 2.20 in ^{F,H}**1**, and it decreases to 2.15 ± 0.02 Å in $^{H,R'}$**1**, in which there is no substituent in the α-position of the pyridine ring. This observation strongly suggests that the bulkiness of the substituent in the α-position of the pyridine ring has a significant and systematic influence on the Fe−N_{py} distance, being longer for bulkier-substituted pyridines. Substitution in the γ-position of the pyridine only provides slight changes in the Fe−N_{py} bond.

As previously reported,[11a] the X-ray structure of the dark red compound ^{H,H}**2**PF_6 is characteristic of a low-spin (LS) iron(II) center, as evidenced by the short Fe−N distances at around 2.0 Å.[15,16] The situation is different for the bis-acetonitrile complex ^{Me,H}**2**SbF_6, whose structure was solved at 300 and 100 K because an evident and reversible change in color from colorless to dark blue was observed when the crystal sample was cooled. Figure 2 shows a representation of the X-ray structure of ^{Me,H}**2**SbF_6, Table 3 collects the experimental details of the crystal-structure determination, and a list of selected bond distances can be found in Table 4. A free acetonitrile molecule is present in the unit cell, and the coordination geometry of the cationic $[Fe(^{Me,H}Pytacn)(CH_3CN)_2]^{2+}$ molecule is the same as in the parent triflato analogues; therefore, it will not be described further. The X-ray structure at 300 K presents an iron(II) center with an average Fe−N distance of 2.20 Å, indicative of a high-spin (HS) electronic configuration (Figure 2).[15b,16a,17] A significant contraction of the unit cell occurs when the temperature is reduced from 300 to 100 K. It corresponds to a unit-cell-volume decrease of ∼7% (from 3365.1 to 3105.9 $Å^3$). This is accompanied by a contraction of the coordination sphere so that the average Fe−N distance at 100 K becomes 2.02 Å, a value typical of a low-spin (LS) Fe^{II}

dx.doi.org/10.1021/ic4004033 | *Inorg. Chem.* 2013, 52, 9229−9244

Table 1. Crystal Data for ^{F,H}1, ^{H,NO2}1, ^{H,NMe2}1, and ^{Me,Me}1

	^{F,H}1	^{H,NO2}1	^{H,NMe2}1	^{Me,Me}1
empirical formula	$C_{16}H_{23}F_7FeN_4O_6S_2$	$C_{16}H_{23}F_6FeN_5O_8S_2$	$C_{18}H_{29}F_6FeN_5O_6S_2$	$C_{18}H_{28}F_6FeN_4O_6S_2$
formula weight	620.35	647.36	645.43	630.41
temperature	100(2) K	100(2) K	100(2) K	100(2) K
wavelength	0.71073 Å	0.71073 Å	0.71073 Å	0.71073 Å
crystal system	monoclinic	monoclinic	monoclinic	orthorhombic
space group	$P2_1/c$	$P2_1/c$	$P2_1/c$	$P2_12_12_1$
unit cell dimensions	a = 15.926(4) Å	a = 9.4350(8) Å	a = 8.745(8) Å	a = 8.8046(14) Å
	α = 90°	α = 90°	α = 90°	α = 90°
	b = 9.434(2) Å	b = 14.8017(12) Å	b = 25.56(2) Å	b = 13.591(2) Å
	β = 115.519(4)°	β = 95.722(2)°	β = 124.53(4)°	β = 90.00°
	c = 17.376(4) Å	c = 17.4272(14) Å	c = 14.522(10) Å	c = 21.920(3) Å
	γ = 90°	γ = 90°	γ = 90°	γ = 90°
volume	2356.0(9) Å^3	2421.7(3) Å^3	2674(4) Å^3	2622.9(7) Å^3
density (calculated)	1.749 g·cm^{-3}	1.776 g·cm^{-3}	1.603 g·cm^{-3}	1.596 g·cm^{-3}
absorption coefficient	0.914 mm^{-1}	0.895 mm^{-1}	0.805 mm^{-1}	0.818 mm^{-1}
F(000)	1264	1320	1328	1296
cell formula units_Z	4	4	4	4
crystal size	0.6 × 0.1 × 0.07 mm	0.35 × 0.30 × 0.12 mm	0.35 × 0.2 × 0.1 mm	0.3 × 0.2 × 0.15 mm
Θ range for data collection	2.36−28.52°	2.169−28.339°	2.332−28.308°	2.39−28.34°
limiting indices	$-21 \le h \le 21$	$-12 \le h \le 12$	$-11 \le h \le 11$	$-11 \le h \le 11$
	$-12 \le k \le 12$	$-19 \le k \le 19$	$-33 \le k \le 32$	$-18 \le k \le 18$
	$-22 \le l \le 22$	$-22 \le l \le 22$	$-19 \le l \le 19$	$-29 \le l \le 29$
reflections collected	34 373	37 799	23 266	40 513
independent reflections	5817	5956	6504	6504
	[R(int) = 0.0752]	[R(int) = 0.0398]	[R(int) = 0.0872]	[R(int) = 0.0327]
completeness to Θ	97.1% (Θ = 28.52°)	99.8% (Θ = 25.242°)	99.9% (Θ = 25.242°)	99.8% (Θ = 28.34)
refinement method	full-matrix least-squares on F^2	full-matrix least-squares on F^2	full-matrix least-squares on F^2	full-matrix least-squares on F^2
data/restraints/parameters	5817/0/327	5956/9/345	6504/0/347	6504/0/339
goodness-of-fit on F^2	1.024	1.056	1.042	1.034
final R indices [$I > 2\sigma(I)$]	$R1$ = 0.0591	$R1$ = 0.0439	$R1$ = 0.0701	$R1$ = 0.0226
	w$R2$ = 0.1498	w$R2$ = 0.1163	w$R2$ = 0.1305	w$R2$ = 0.0554
R indices (all data)	$R1$ = 0.1133	$R1$ = 0.0532	$R1$ = 0.1098	$R1$ = 0.0254
	w$R2$ = 0.1764	w$R2$ = 0.1233	w$R2$ = 0.1450	w$R2$ = 0.0565
largest diff peak and hole	1.750 and −0.701 e·Å^{-3}	1.862 and −0.844 e·Å^{-3}	0.885 and −0.473 e·Å^{-3}	0.361 and −0.207 e·Å^{-3}

Table 2. Selected Bond Lengths (Å) and Angles (°) for ^{F,H}1, ^{H,NO2}1, ^{H,NMe2}1, and ^{Me,Me}1

^{F,H}1		^{H,NO2}1		^{H,NMe2}1		^{Me,Me}1	
Fe−N1	2.196(4)	Fe−N1	2.183(2)	Fe−N1	2.153(4)	Fe−N1	2.2112(13)
Fe−N2	2.201(4)	Fe−N4	2.208(2)	Fe−N3	2.220(4)	Fe−N2	2.1720(13)
Fe−N3	2.218(4)	Fe−N5	2.220(2)	Fe−N4	2.219(4)	Fe−N3	2.2419(13)
Fe−N4	2.211(4)	Fe−N3	2.188(2)	Fe−N5	2.258(4)	Fe−N4	2.2247(13)
Fe−O2	2.043(3)	Fe−O3	2.0365(19)	Fe−O1	2.093(3)	Fe−O1	2.1910(12)
Fe−O4	2.149(3)	Fe−O6	2.1415(19)	Fe−O4	2.151(3)	Fe−O4	2.0513(11)
N1−Fe−N2	76.11(13)	N4−Fe−O3	92.16(8)	N1−Fe−N3	78.65(13)	N1−Fe−N2	76.37(5)
N1−Fe−N4	92.43(15)	N4−Fe−N5	80.79(8)	N1−Fe−N5	94.28(13)	N1−Fe−N3	107.38(5)
N1−Fe−O4	95.24(13)	N1−Fe−O3	110.21(8)	N1−Fe−O4	93.34(13)	N1−Fe−O1	86.36(5)
N1−Fe−O1	106.49(13)	N1−Fe−O6	84.04(8)	N1−Fe−O1	108.94(13)	N1−Fe−O4	107.11(5)
N4−Fe−N2	79.99(14)	N4−Fe−N3	80.29(8)	N5−Fe−N3	79.52(14)	N2−Fe−N4	80.28(5)
N4−Fe−N3	80.53(16)	N5−Fe−N3	81.38(8)	N5−Fe−N4	80.40(14)	N3−Fe−N4	79.52(5)
N2−Fe−O4	92.66(14)	N4−Fe−O6	98.53(8)	N3−Fe−O4	94.37(14)	N4−Fe−O1	86.81(5)
N4−Fe−O1	96.29(14)	N5−Fe−O3	96.28(8)	N5−Fe−O1	93.74(14)	N4−Fe−O4	97.19(5)
N3−Fe−O1	96.35(15)	N1−Fe−N5	94.71(8)	N4−Fe−O1	92.49(13)	N2−Fe−O1	100.62(5)
N2−Fe−N3	80.82(16)	N1−Fe−N3	77.31(8)	N3−Fe−N4	79.67(14)	N2−Fe−N3	80.36(5)
N3−Fe−O4	88.74(14)	N3−Fe−O6	93.64(8)	N4−Fe−O4	89.67(13)	N3−Fe−O4	93.84(5)
O4−Fe−O1	90.60(13)	O3−Fe−O6	88.67(8)	O4−Fe−O1	91.15(14)	O1−Fe−O4	84.61(5)

center (Table 4).[15b,16a,17] This contraction in bond distance is indicative of a spin transition in the solid state from high- (300 K) to low-spin (100 K).[18] The complete spin transition was also evident by measurement of the molar susceptibility (χ_m) as a function of the temperature using a SQUID magnetometer (Figure S3). ^{Me,H}**2**SbF_6 presents a gradual spin-crossover occurring over a temperature range of approximately 100 K and centered at around 170 K.

dx.doi.org/10.1021/ic4004033 | Inorg. Chem. 2013, 52, 9229−9244

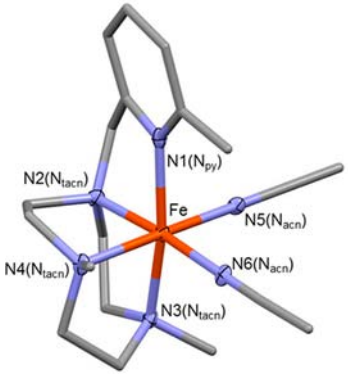

	100 K	300 K
Fe-N$_{py}$	2.074	2.223
Fe-N$_{tacn}$	2.030	2.214
Fe-N$_{acn}$	1.944	2.155

Figure 2. Representation of the cationic part of the X-ray structure of ^{Me,H}**2**$SbF_6 \cdot CH_3CN$ at 100 K. The table shows the Fe−N_{py}, the average Fe−N_{tacn}, and the average Fe−N_{acn} bond lengths for this compound at a given temperature (100 and 300 K). Hydrogen atoms and the noncoordinated acetonitrile molecule found in the unit cell have been omitted for clarity.

^{1}H NMR Spectroscopy. As representative examples of the family of bis-triflato complexes, ^{1}H NMR spectra of ^{H,H}**1**, ^{Me,H}**1**, ^{H,NO2}**1**, and ^{H,NMe2}**1** in CD_2Cl_2 are depicted in Figure 3. Figures S4 and S5 in the Supporting Information collect the ^{1}H NMR spectra of all complexes ($^{R,R'}$**1**). These compounds exhibit spectral windows that expand from −40 to 200 ppm, which is

Table 4. Selected Bond Lengths (Å) and Angles (°) for ^{Me,H}2$SbF_6 \cdot CH_3CN$ at 100 and 300 K

^{Me,H}2$SbF_6 \cdot CH_3CN$ (100 K)		^{Me,H}2$SbF_6 \cdot CH_3CN$ (300 K)	
Fe−N1	2.075(5)	Fe−N1	2.251(6)
Fe−N2	1.986(5)	Fe−N2	2.179(6)
Fe−N3	2.039(5)	Fe−N3	2.213(6)
Fe−N4	2.064(5)	Fe−N4	2.248(6)
Fe−N5	1.946(5)	Fe−N5	2.188(6)
Fe−N6	1.942(5)	Fe−N6	2.194(6)
N1−Fe−N2	82.9(2)	N1−Fe−N2	2.191(6)
N1−Fe−N4	94.2(2)	N1−Fe−N4	2.182(7)
N1−Fe−N5	87.5(2)	N1−Fe−N5	2.218(6)
N1−Fe−N6	101.2(2)	N1−Fe−N6	2.234(6)
N3−Fe−N2	84.8(2)	N3−Fe−N2	2.167(7)
N3−Fe−N4	84.9(2)	N3−Fe−N4	2.184(6)
N3−Fe−N5	93.1(2)	N3−Fe−N5	2.175(4)
N3−Fe−N6	91.1(2)	N3−Fe−N6	2.181(6)
N2−Fe−N4	85.0(2)	N2−Fe−N4	2.221(6)
N2−Fe−N5	93.8(2)	N2−Fe−N5	2.231(7)
N5−Fe−N6	88.6(2)	N5−Fe−N6	2.184(7)
N4−Fe−N6	92.6(2)	N4−Fe−N6	2.172(7)

Table 3. Crystal Data for ^{Me,H}2$SbF_6 \cdot CH_3CN$ at 100 and 300 K

	^{Me,H}2$SbF_6 \cdot CH_3CN$ (100 K)	^{Me,H}2$SbF_6 \cdot CH_3CN$ (300 K)
empirical formula	$C_{21}H_{35}F_{12}FeN_7Sb_2$	$C_{21}H_{35}F_{12}FeN_7Sb_2$
formula weight	912.91	912.91
temperature	100(2) K	300(2) K
wavelength	0.71073 Å	0.71073 Å
crystal system	monoclinic	monoclinic
space group	$P2_1/c$	$P2_1/c$
unit cell dimensions	a = 13.0482(17) Å	a = 13.3058(18) Å
	α = 90°	α = 90°
	b = 12.2015(16) Å	b = 12.4573(17) Å
	β = 101.023(2)°	β = 100.276(2)°
	c = 19.875(3) Å	c = 20.633(3) Å
	γ = 90°	γ = 90°
volume	3105.9(7) Å^3	3365.1(8) Å^3
density (calculated)	1.952 g·cm^{-3}	2.802 g·cm^{-3}
absorption coefficient	2.286 mm^{-1}	2.110 mm^{-1}
F(000)	1784	1784
cell formula units_Z	4	4
crystal size	0.35 × 0.35 × 0.08 mm	0.35 × 0.35 × 0.08 mm
Θ range for data collection	2.062−28.358°	2.257−28.271°
limiting indices	$-17 \le h \le 17$	$-17 \le h \le 17$
	$-16 \le k \le 16$	$-16 \le k \le 16$
	$-26 \le l \le 26$	$-27 \le l \le 27$
reflections collected	46 648	51 823
independent reflections	7689	8279
	[R(int) = 0.0779]	[R(int) = 0.0842]
completeness to Θ	99.9% (Θ = 25.242°)	99.9% (Θ = 25.242°)
refinement method	full-matrix least-squares on F^2	full-matrix least-squares on F^2
data/restraints/parameters	7689/0/394	8279/0/394
goodness-of-fit on F^2	1.246	1.006
final R indices [$I > 2\sigma(I)$]	$R1$ = 0.0634	$R1$ = 0.0513
	w$R2$ = 0.1204	w$R2$ = 0.1219
R indices (all data)	$R1$ = 0.0799	$R1$ = 0.1087
	w$R2$ = 0.1253	w$R2$ = 0.1494
largest diff peak and hole	1.599 and −1.352 e·Å^{-3}	1.166 and −0.689 e·Å^{-3}

dx.doi.org/10.1021/ic4004033 | Inorg. Chem. 2013, 52, 9229−9244

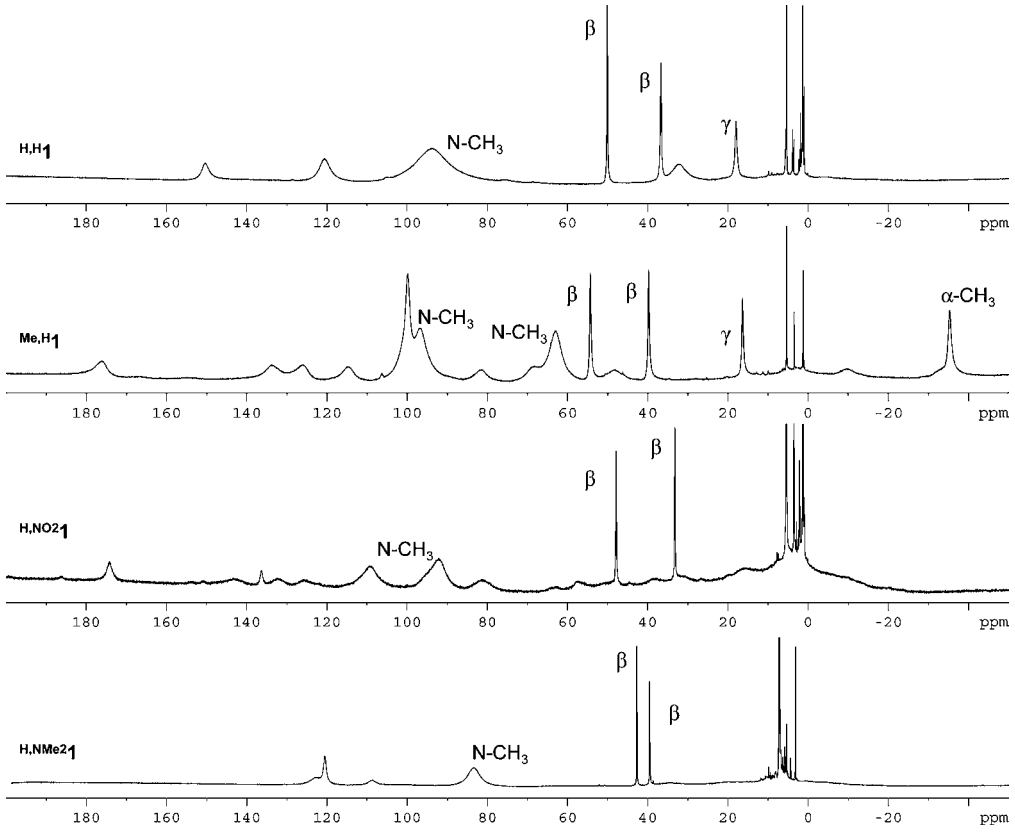

Figure 3. ^{1}H NMR spectra (400 MHz) of ^{H,H}**1**, ^{Me,H}**1**, ^{H,NO2}**1**, and ^{H,NMe2}**1** in CD_2Cl_2.

indicative of octahedral $t_{2g}^{4}e_g^{2}$ Fe^{II} paramagnetic species. Spectra show mainly very broad signals because of the close proximity of the corresponding protons to the paramagnetic center. Along this line, in most of the cases the spectra are rather simple, with a relatively small number of signals, suggesting that some protons give signals that are too broad to be effectively observed because of fast relaxation. Lowering the temperature causes a narrowing of the NMR signals as exemplified for complex ^{Me,H}**1** (Figure S6), whose protons exhibit chemical shifts linearly dependent on $1/T$, which is characteristic of a Curie behavior (Figure S7).

In spite of the width of the NMR signals at room temperature, it is possible to clearly identify β and γ protons of the pyridine, which appear as relatively sharp signals (Table 5). They can be assigned on the basis of their relative integration, by comparison of the spectra along the whole series of complexes and because polypyridyl Fe^{II} complexes present typical NMR patterns.[15c,16,19] This assignment explains the absence of a sharp signal at 15−20 ppm, corresponding to the γ proton for compounds $^{H,R'}$**1** and ^{Me,Me}**1**, which bear a substituent in the *para*-position of the pyridine ring and the lack of the two sharp signals between 30 and 70 ppm in the ^{1}H NMR spectrum of ^{H,OMe}**1**, for which the pyridine ring presents methyl groups in the two β-positions. Assignment of the α-methylpyridine group in ^{Me,Me}**1** and ^{Me,H}**1** can also be made because of the characteristic paramagnetic upfield shift of these protons arising from Fermi contact interactions between protons and the ferrous center, dominated by a spin polarization mechanism (Figure S5).[16a,20] Resonances belonging to the N−CH_3 groups could be easily identified in the spectra of ^{H,H}**1** and ^{H,NMe2}**1** as a very broad signal between 80 and 100 ppm on the basis of their relative integration. The two

Table 5. ^{1}H NMR Chemical Shifts (ppm) for β and γ Protons of the Pyridine Ring of Complexes $^{R,R'}$1 in CD_2Cl_2

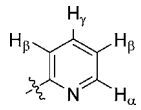

complex	H_β	H_β	H_γ
^{H,H}**1**	49.2	36.3	17.7
^{H,NMe2}**1**	42.7	39.5	
^{H,OMe}**1**			
^{H,Me}**1**	47.7	35.6	
^{H,Cl}**1**	47.8	33.8	
^{H,CO2Et}**1**	49.7	34.9	
^{H,NO2}**1**	47.8	33.2	
^{Me,H}**1**	53.1	38.8	16.5
^{Me,Me}**1**	52.6	39.0	
^{Cl,H}**1**	60.3	32.4	18.6
^{F,H}**1**	68.8	29.7	18.5

N−CH_3 groups of each [Fe(Pytacn)] unit are chemically nonequivalent, but they accidentally overlap in the spectra of ^{H,H}**1**. This situation is changed in the spectra of ^{Me,H}**1** and ^{H,NO2}**1**, where the two N−CH_3 groups appear as two different signals at 65/95 and 95/110 ppm (Figure 3), and also in the spectra of ^{R,H}**1** (R = Me, Cl, and F in Figure S5) and $^{H,R'}$**1** (R′ = OMe, Me, Cl, and CO_2Et in Figure S4) in CD_2Cl_2.

^{1}H NMR spectra of $^{R,R'}$**1** were also measured in CD_3CN (Figures 4 and 5 and S8−S11). Similar to what is reported for other iron(II) complexes,[15b,21] this solvent acts as a coordinating ligand, and it displaces triflate groups to form solvato complexes $[Fe(^{R,R'}Pytacn)(CH_3CN)_2]^{2+}$ ($^{R,R'}$**2**OTf), in

dx.doi.org/10.1021/ic4004033 | Inorg. Chem. 2013, 52, 9229−9244

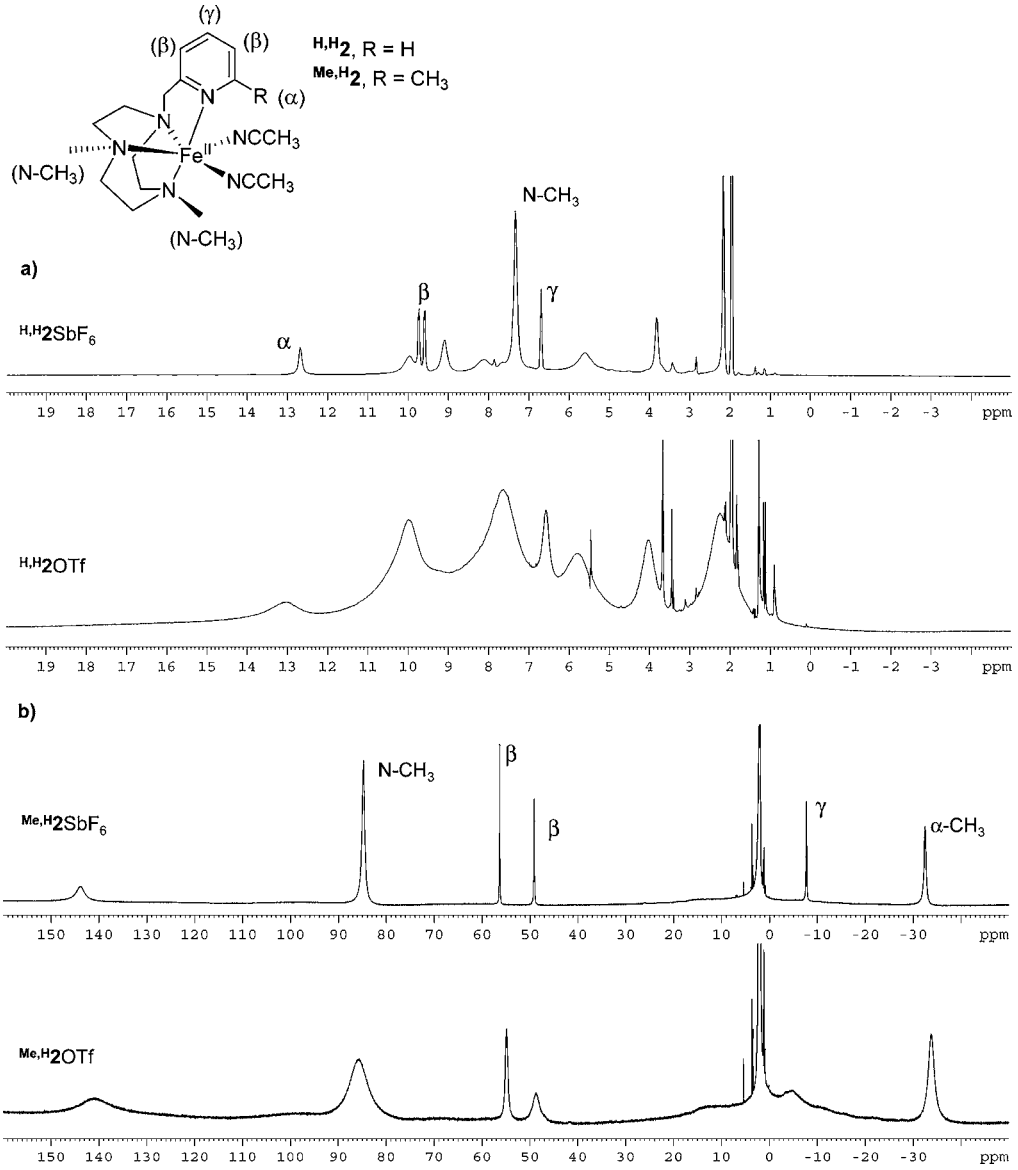

Figure 4. (a) ^{1}H NMR spectra (400 MHz) of ^{H,H}**2**SbF_6 and ^{H,H}**1** in CD_3CN. The latter affords the bis-acetonitrile complex ^{H,H}**2**OTf upon being dissolved. The partial assignation of the ^{1}H NMR signals for complex ^{H,H}**2**SbF_6 was based on integration values and COSY experiment (Figure S8b). ^{1}H NMR spectra (400 MHz) of ^{Me,H}**2**SbF_6 and ^{Me,H}**1** in CD_3CN. The latter affords the bis-acetonitrile complex ^{Me,H}**2**OTf upon being dissolved. For complex ^{Me,H}**2**SbF_6, the assignation was made by comparison with similar complexes described in the literature[16a,22] and according to the integration values (Figure S9).

which two acetonitrile molecules and the tetradentate $^{R,R'}$-Pytacn ligand constitute the coordination sphere of the iron(II) center. This phenomenon was confirmed by comparing the ^{1}H NMR spectra of ^{H,H}**1** and ^{Me,H}**1** in CD_3CN (^{H,H}**2**OTf and ^{Me,H}**2**OTf) with those of the synthetically isolated bis-acetonitrile complexes ^{H,H}**2**SbF_6 and ^{Me,H}**2**SbF_6 (Figure 4). For these two compounds, the ^{1}H NMR spectrum exhibited much sharper signals than the corresponding bis-triflato complexes ^{H,H}**1** and ^{Me,H}**1** in CD_3CN, but chemical shifts and relative integrals were essentially the same. This observation is indicative of a fast exchange between triflate and acetonitrile binding, which gives rise to broader signals for ^{H,H}**2**OTf and ^{Me,H}**2**OTf.[10a]

The spectral window of the ^{1}H NMR spectrum of each complex in CD_3CN reflects the spin state of $^{R,R'}$**2**OTf. Important differences arise upon analysis of these NMR spectra so that the complexes might be classified into two categories: complexes without any substituent in the α-position (class I) and complexes with a substituent in this position (class II).

On the one hand, class I complexes, that is $^{H,R'}$**2**OTf, exhibit a compact spectral window compared to their bis-triflato counterparts ($^{H,R'}$**1**). It expands from 0 to 15 ppm, except for ^{H,NMe2}**2**OTf, which shows signals up to 45 ppm (Figure S10). The contraction of the spectral window is related to a modification of the electronic properties of the iron complex, which becomes mainly LS upon substitution of the triflate anions by acetonitrile ligands. This has been previously observed for other iron complexes[10a,15a,d,23], and it can be explained by simple crystal field theory because the acetonitrile ligand is a stronger ligand field than triflate anion. Qualitative analysis of the NMR spectra allows the evaluation of the relative contribution of the HS state. It is particularly interesting to notice that complex ^{H,NO2}**2**OTf, with a nitro group in the γ-position, does not show signals above 11 ppm, which indicates

dx.doi.org/10.1021/ic4004033 | Inorg. Chem. 2013, 52, 9229−9244

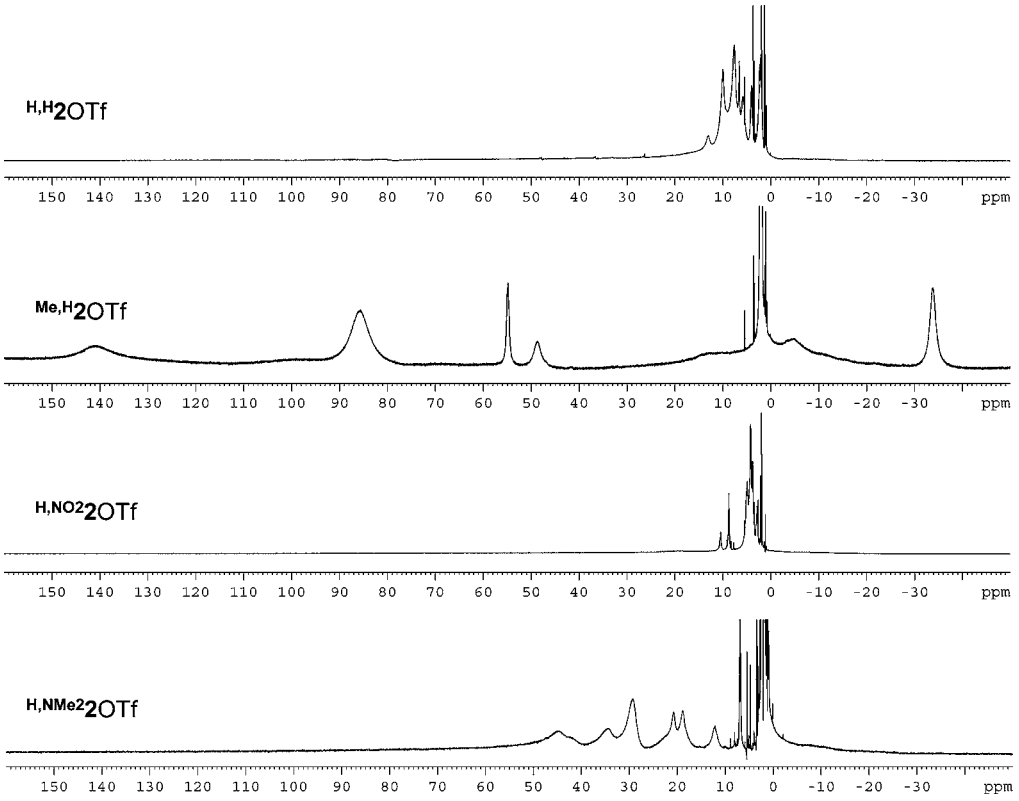

Figure 5. ^{1}H NMR spectra (400 MHz) of ^{H,H}**1**, ^{Me,H}**1**, ^{H,NO2}**1**, and ^{H,NMe2}**1** in CD_3CN. The triflate anions are replaced by acetonitrile molecules, thus, the bis-acetonitrile complexes ^{H,H}2OTf, ^{Me,H}2OTf, ^{H,NO2}2OTf, and ^{H,NMe2}2OTf are formed in solution.

Table 6. Selected Physical Data for $^{R,R'}$2OTf[a]

	λ_{max}, nm (ε, $M^{-1}\cdot cm^{-1}$)			
complex	$\pi-\pi^*$	MLCT	d−d	μ_{eff}, μ_B[b]
^{H,H}2OTf	239 (13 900)	385 (3200)	550 (65)	1.26
^{H,NMe2}2OTf	240 (> 20 000)	327 (4700)	540 sh (100)	2.62
^{H,OMe}2OTf	250 (13300)	370 (5400)	547 (120)	2.09
^{H,Me}2OTf	240 (10500)	370 (2900)	553 (70)	1.24
^{H,Cl}2OTf	241 (15800)	403 (3900)	547 (45)	1.71
^{H,CO2Et}2OTf	275 (6150)	455 (6100)		0.78
^{H,NO2}2OTf	231 (14000)	526 (2400)		0
^{Me,H}2OTf	267 (5100)	340 (255)		4.95
^{Me,Me}2OTf	260 (4700)	344 (220)		4.75
^{Cl,H}2OTf	269 (7000)	410(950)		4.87
^{F,H}2OTf	237 (5600), 254 (5600)	368 (900)	578 (14)	4.63

[a]Compounds $^{R,R'}$2OTf were prepared by dissolving the bis-triflato complexes $^{R,R'}$**1** in CH_3CN or CD_3CN. [b]Determined by the Evans' method.

that in this case the compound is purely diamagnetic and must be described as a pure LS iron(II) center (Figure 5). Instead, for ^{H,NMe2}2OTf, which has a strongly electron-donating dimethylamino substituent in the γ-position, there is an important influence of the HS state, and the spectral window expands up to 45 ppm (Figure 5). Thus, it seems clear that the substituent in the *para*-position of the pyridine directly influences the electronic properties of the iron(II) center. In contrast, class II catalysts, that is $^{R,R'}$2OTf, where R = Me, Cl, or F, show spectral windows that expand from 0 to 150 ppm, indicating a HS configuration of the iron(II) center in acetonitrile (Figure S11).

The different spin states of the iron(II) center in class I and class II bis-acetonitrile complexes, evidenced by NMR spectroscopy, could be quantified by measuring their effective magnetic moment (μ_{eff}) using the Evans' method (see below).

Effective Magnetic Moment. The measurement of the effective magnetic moment (μ_{eff}) allows the quantification of the contribution of the LS and HS states in iron(II) complexes. This information is specially important in the present family of complexes, for which both spin states are close in energy. Values of μ_{eff} for $^{R,R'}$2OTf were measured using the Evans' NMR method by dissolving $^{R,R'}$**1** in CD_3CN (Table 6).

For class I complexes, μ_{eff} values are clearly influenced by the electronic properties of the group in the γ-position. As detailed in Table 6, μ_{eff} increases when the electron-donating properties of this substituent are increased. The extreme cases correspond to ^{H,NO2}2OTf, with a highly electron-withdrawing group and no

dx.doi.org/10.1021/ic4004033 | Inorg. Chem. 2013, 52, 9229−9244

effective magnetic moment, indicative of a LS Fe^{II} (in agreement with its diamagnetic ^{1}H NMR spectrum) and ^{H,NMe_2}**2**OTf, with the strongest electron-donating γ-substituent and a μ_{eff} of 2.62 μ_B, implying a significant population of the HS state. The influence of the γ-substituent in the μ_{eff} is clearly observed by the good correlation of this value with the corresponding Hammett σ_p constant (Figure 6a). These values

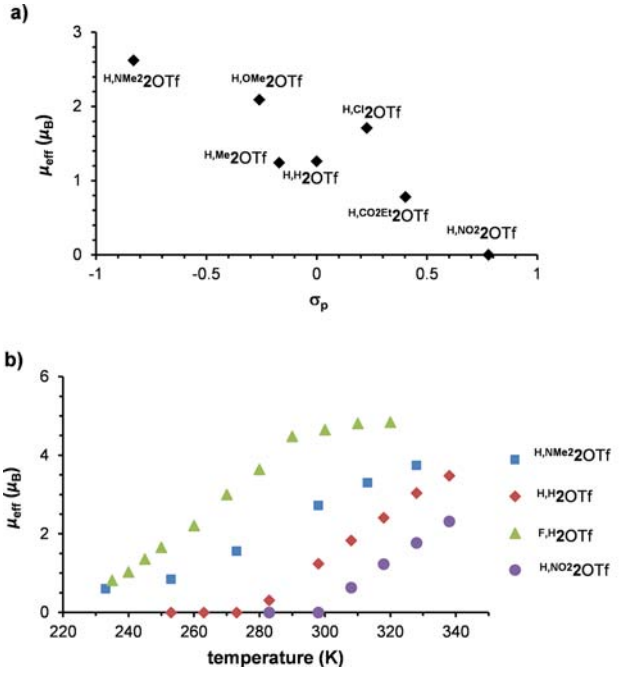

Figure 6. (a) Representation of the effective magnetic moment of $^{H,R'}$**2**OTf in CD_3CN at 298 K in front of the Hammett constants. (b) Representation of the effective magnetic moment of ^{H,H}**2**OTf, ^{F,H}**2**OTf, ^{H,NO_2}**2**OTf, and ^{H,NMe_2}**2**OTf as a function of temperature. $^{R,R'}$**2**OTf complexes were obtained by dissolving $^{R,R'}$**1** in CD_3CN. The effective magnetic moment was measured in CD_3CN solutions using the Evans' method.

fully agree with the increased spectral window of the ^{1}H NMR spectra upon increasing the electron-donating abilities of the *para*-substituent (Figure S10). The effect of the pyridine substitution on the μ_{eff} can be understood on the basis of simple ligand field theory, by assuming that this value reflects different stages of a spin transition equilibrium. According to this theory, the magnitude of the ligand field (i.e., the t_{2g}-e_g orbital splitting) is higher when increasing the π-acceptor character of the ligands. Introduction of NO_2 and NMe_2 groups into the pyridine causes, respectively, a decrease and an increase of the energy of the pyridine π orbitals, with respect to the hydrogen-, methyl-, or chloro-substituted ligands. Therefore, the NO_2 group makes the pyridine a better π-acceptor, while the opposite happens with the NMe_2 group. Overall, electron-withdrawing groups increase the ligand field, favoring the LS state, while the opposite occurs for electron-releasing groups, which populate the HS state.

Class I complexes exhibit an incomplete spin-crossover phenomenon with the temperature, as previously observed for structurally related iron(II) complexes.[21a] This behavior was studied for complexes ^{H,H}**2**OTf, ^{H,NMe_2}**2**OTf, and ^{H,NO_2}**2**OTf, as representative examples of this class, bearing a hydrogen atom, an electron-donating group, and an electron-withdrawing group in the γ-position of the pyridine, respectively (Figure 6b). Taking 298 K as the initial temperature, it was observed that increasing the temperature to 338 K caused a significant increase in the μ_{eff}. The opposite was observed upon cooling. As stated above, ^{H,NO_2}**2**OTf already has a diamagnetic behavior at room temperature, while for ^{H,H}**2**OTf the pure LS state was reached at 273 K. In contrast, complete conversion to the LS state does not occur for ^{H,NMe_2}**2**OTf in the temperature range accessible with acetonitrile, but at 233 K a small μ_{eff} of 0.8 μ_B was measured, which is indicative of a major contribution of the LS state.

The situation is completely different for compounds belonging to class II, which bear a substituent in the α-position of the pyridine ring (^{R,H}**2**OTf). The measured μ_{eff} values of 4.80 ± 0.17 μ_B are very close to the theoretical spin-only value of 4.90 μ_B of a HS iron(II) center with four unpaired electrons. This result fully agrees with the paramagnetism observed by ^{1}H NMR for the compounds in this class (Figure S11). It is likely that the α-substituent in the pyridine sterically interacts with the iron center, which disfavors the formation of the shorter Fe−N bond characteristic of the LS configuration.[16a] However, it is interesting to notice that the μ_{eff} value measured for ^{F,H}**2**OTf is slightly lower (4.63 μ_B) than what would be expected for a pure HS center with four unpaired electrons. It was observed that the μ_{eff} values for ^{F,H}**2**OTf decreased upon lowering the temperature, which is consistent with a spin transition phenomenon in solution. Ranges of μ_{eff} from 4.77 μ_B at 320 K to 0.92 μ_B at 235 K (Figure 6b) indicate an almost complete crossover, reminiscent to that observed for structurally related systems.[21a,b,22] This spin transition could also be followed by UV−vis spectroscopy (Figure 8). In order to exclude the occurrence of the decoordination of the 6-fluoropyridine and the posterior coordination of acetonitrile solvent molecules upon lowering the temperature, which could also explain the change in the spin state, we carried out variable-temperature ^{19}F NMR (298 to 230 K) experiments. No significant changes in the ^{19}F NMR spectra were observed in the temperature range studied, and only a single sharp signal at −79 ppm assigned to the noncoordinated triflate counterions was observed.[21a,c] If decoordination of 6-fluoropyridine occurred, the presence of a fluorine sharp signal around −65 ppm would be expected.[24] The fluorine substituent in the sixth position of the pyridine ring was not detected, likely because pyridine coordination places this atom in close proximity to the paramagnetic iron(II) center. This causes short relaxation times and significant signal broadening, a phenomenon that has been previously reported in structurally related complexes with fluoro α-substituted pyridine-based ligands.[21c] Spin-crossover in solution was not observed for the other class II complexes, that is, ^{Me,H}**2**OTf, ^{Cl,H}**2**OTf, and ^{Me,Me}**2**OTf, which remain HS when the temperature is decreased.

UV−Vis Spectroscopy. The UV−vis spectra of the bis-acetonitrile complexes $^{R,R'}$**2**OTf, formed by dissolving the corresponding bis-triflato complexes $^{R,R'}$**1** in acetonitrile, were analyzed to obtain further information about the electronic structure of the complexes (Table 6 and Figure 7).

Compound ^{H,H}**2**OTf is a prototypical example of class I complexes. The UV−vis spectrum of this compound is characterized by intense bands at 239 (ε = 13 900 $M^{-1}\cdot cm^{-1}$), 385 (ε = 3200 $M^{-1}\cdot cm^{-1}$), and a relatively weak band at 550 nm (ε = 65 $M^{-1}\cdot cm^{-1}$), which is responsible for the pink-yellowish color of the solution (Figure 7 and Table 6). By analogy to the UV−vis spectra of other iron(II) complexes of pyridine-alkylamino ligands,[21a,b,25] the two high-intensity

dx.doi.org/10.1021/ic4004033 | Inorg. Chem. 2013, 52, 9229−9244

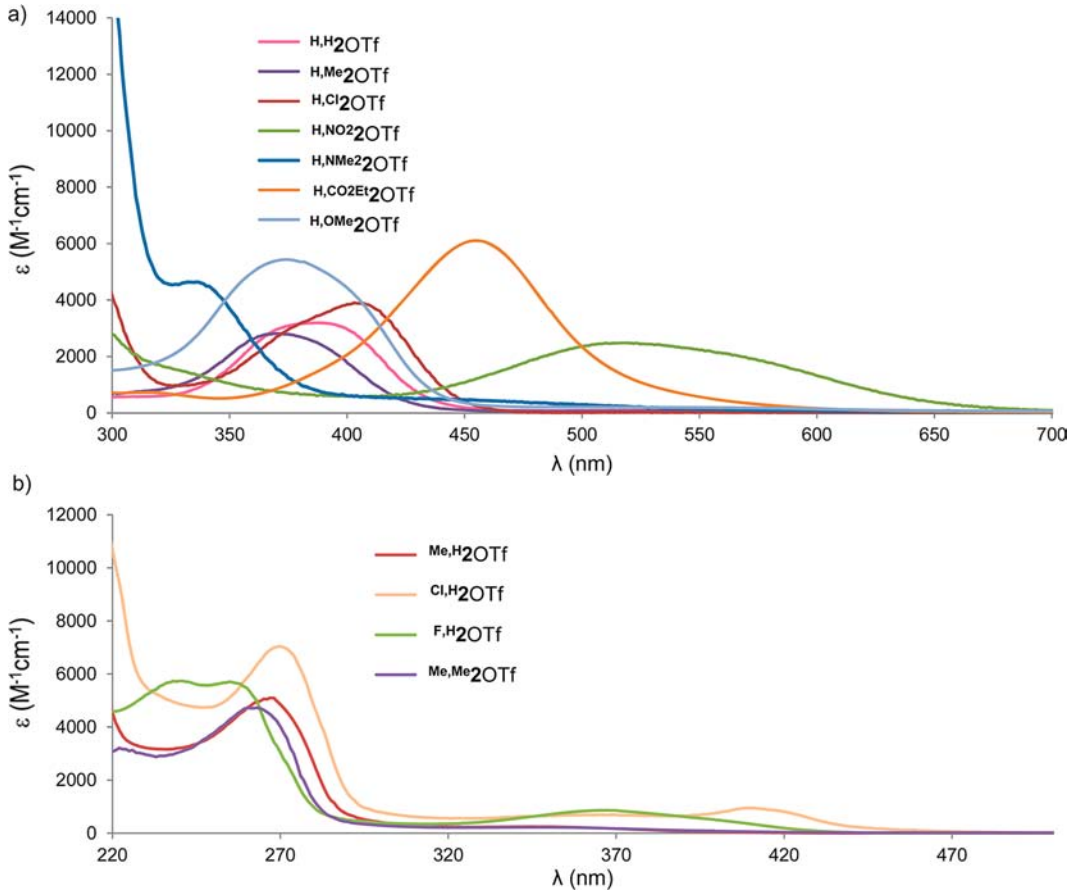

Figure 7. (a) UV−vis spectra (298 K) in acetonitrile of complexes $^{H,R'}$**2**OTf. (b) UV−vis spectra (298 K) in acetonitrile of $^{R,R'}$**2**OTf where R = Me, Cl, or F. $^{R,R'}$**2**OTf complexes were obtained upon dissolving $^{R,R'}$**1** in acetonitrile.

bands in the UV region can be assigned to a ligand-centered $\pi-\pi^*$ transition and to a metal-to-ligand charge transfer (MLCT), respectively. The latter arises from a transition between the iron(II) t_{2g} orbitals and the π^* pyridine orbitals,[26] thus, being more intense for low-spin iron(II) compounds. In the particular case of ^{H,H}**2**OTf, the intensity of the MLCT band is consistent with a LS iron(II) center. Finally, the low-intensity broad band at 550 nm is assigned to a d−d transition that is characteristic of an octahedral LS iron(II) complex ($^1T_1 \leftarrow {}^1A_1$).

The position of the intense MLCT band ($\varepsilon \approx 2400-6100$ $M^{-1}\cdot cm^{-1}$) is directly related to the electronic properties of the γ-substituent. An increase in the electron-withdrawing character of the γ-group causes a bathochromic shift (Figure 7a). Thus, the energy of this band decreases in the following order: NMe_2 > OMe ≈ Me > H > Cl > CO_2Et > NO_2. This phenomenon has been previously observed for other iron complexes, [21a] and it can be rationalized by the tuned π-acceptor character of the pyridine ring. The shift in the λ_{max} is so significant for ^{H,NO2}**2**OTf and ^{H,CO2Et}**2**OTf that the weak d−d transition is masked by the overlap with this intense MLCT band.

For class II catalysts, the UV−vis spectrum of ^{Me,H}**2**OTf, which is very similar to that of ^{Cl,H}**2**OTf and ^{Me,Me}**2**OTf, is taken as the reference. This complex exhibits a band at 267 nm ($\varepsilon \sim 5100$ $M^{-1}\cdot cm^{-1}$), corresponding to a ligand-centered $\pi-\pi^*$ transition and a shoulder at 340 nm ($\varepsilon \sim 255$ $M^{-1}\cdot cm^{-1}$) that is related to a MLCT. The low ε value for the latter is characteristic of a HS iron(II) center (Figure 7b).[25a,26a]

Compound ^{F,H}**2**OTf has a slight contribution of the LS state at room temperature, as evidenced by the presence of a low-intensity band at 578 nm in its UV−vis spectrum, which strongly resembles that d−d transition described above for LS iron(II) complexes (Figure 8). The intensity of this band, as well as that of MLCT, and the $\pi-\pi^*$ transitions at 237 and 368 nm depend on the temperature. Lowering the temperature results in an increase of their molar absorptivity without saturation in the temperature range studied (from 20 to −40 °C) (Figure 8). This behavior indicates a spin-crossover

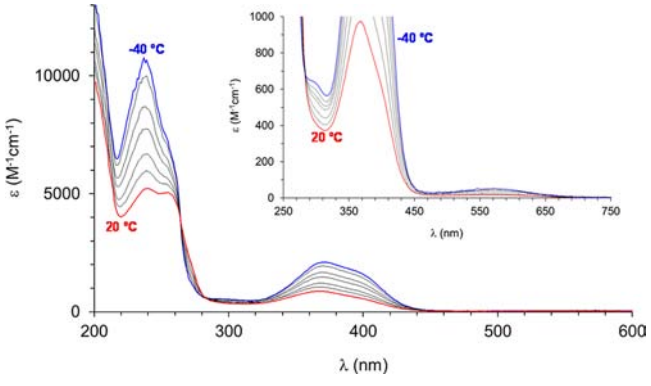

Figure 8. UV−vis spectra of ^{F,H}**1** in CH_3CN at different temperatures (from 20 to −40 °C). The triflate anions are replaced by acetonitrile molecules, thus, the bis-acetonitrile complex ^{F,H}**2**OTf is formed in solution.

dx.doi.org/10.1021/ic4004033 | Inorg. Chem. 2013, 52, 9229−9244

Table 7. Oxidation of Cyclohexane and *cis*-Cyclooctene with H_2O_2 Using Complexes $[Fe(OTf)_2(^{R,R'}Pytacn)]$ ($^{R,R'}$**1**) as Catalysts[a]

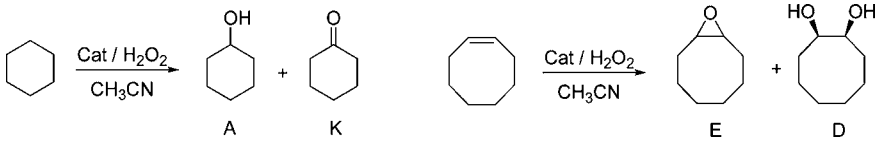

catalyst	H_2O_2 (equiv)	cyclohexane A + K[b] (A/K)[c]	cyclooctene D + E[d] (D/E)[e]	$^{16}O^{18}O$[f]	^{18}O[g]
^{H,H}**1**	10	6.5 (12.3)[11a]	8.1 (1.0)[11a]	97	77
	100	39 (2.6)[11a]	99 (1.0)[11a]		
^{H,NMe2}**1**	10	4.3 (8.9)[27]	8.2 (2.3)	95	74
	100	31 (3.8)	69 (1.4)		
^{H,OMe}**1**	10	6.2 (10.2)[27]	7.6 (1.1)	95	71
	100	47 (2.8)	83 (1.5)		
^{H,Me}**1**	10	6.5 (10.5)[27]	9.3 (2.6)	97	72
	100	48 (2.3)	85 (1.0)		
^{H,Cl}**1**	10	5.9 (8.3)[27]	9.5 (1.5)	97	67
	100	40 (4.3)	85 (2.1)		
^{H,CO2Et}**1**	10	5.7 (9.2)[27]	8.2 (1.5)	97	63
	100	43 (3.2)	82 (1.2)		
^{H,NO2}**1**	10	5.3 (8.1)[27]	7.8 (1.5)	99	66
	100	34 (3.9)	50 (1.1)		
^{Me,H}**1**	10	7.6 (10.2)[11a]	7.1 (5.5)[11a]	78	5
	100	64 (4.3)[11a]	86 (6.2)[11a]		
^{Me,Me}**1**	10	6.1 (9.3)[27]	8.6 (5.2)	80	4
	100	60 (5.1)	81 (3.5)		
^{Cl,H}**1**	10	6.8 (6.7)[27]	8.4 (2.6)	80	9
	100	28 (3.0)	63 (4.7)		
^{F,H}**1**	10	5.9 (8.3)[27]	7.5 (0.8)	89	4
	100	26 (2.7)	73 (1.0)		

[a]1000 equiv of substrate (100 equiv for isotope labeling studies) with respect to catalyst. Final catalyst concentration = 1 mM. Reactions were performed by slow-syringe-pump addition over 30 min of an acetonitrile solution of H_2O_2 (10 or 100 equiv) into a solution of catalyst and substrate at room temperature. [b]Turnover number (mols of products/mols of catalyst), A = cyclohexanol, K = cyclohexanone. [c]A/K = mols of alcohol/mols of ketone. [d]Turnover number (mol product/mol catalyst), D = *syn*-cyclooctane-1,2-diol, E = cyclooctene epoxide. [e]D/E = mols of diol/mols of epoxide. [f]Percentage of *syn*-diol $^{16}O^{18}O$-labeled when the oxidation of cyclooctene was carried out in the presence of 1000 equiv of $H_2{}^{18}O$. [g]Percentage of epoxide ^{18}O-labeled when the oxidation of cyclooctene was carried out in the presence of 1000 equiv of $H_2{}^{18}O$.

phenomenon from HS to LS upon lowering the temperature, which was further corroborated by measurement of the effective magnetic moment (see Figure 6b).

Catalytic Oxidations. In order to evaluate the electronic/steric influence imposed by the Pytacn-based ligands in the catalytic activity of the corresponding $[Fe(OTf)_2(^{R,R'}Pytacn)]$ complexes ($^{R,R'}$**1**), we have tested their behavior as catalysts in oxidation reactions using H_2O_2 as the oxidant. In particular, we have targeted the oxidation of cyclohexane and *cis*-cyclooctene as model substrates for C−H bond and C═C bond oxidation reactions (Table 7). Indeed, in previous work, the catalytic activity of $^{R,R'}$**1** in some of these reactions has been studied under very particular conditions.[11a,27]

In a typical experiment, 10−100 equiv of H_2O_2 diluted in acetonitrile was delivered via syringe pump for 30 min into an acetonitrile solution containing the iron catalyst (1 equiv) and the substrate (100−1000 equiv). The final concentrations of the reactants were 1 mM catalyst, 10−100 mM H_2O_2, and 100 mM−1 M substrate. Oxidant-limiting conditions were used in all the experiments in order to limit product overoxidation.

The oxidation of cyclohexane with 10 equiv of H_2O_2 catalyzed by complexes $^{R,R'}$**1** afforded excellent conversion of H_2O_2 into oxidation products (cyclohexanol and cyclohexanone) that ranged from 43 to 76%.[27] Remarkably, large alcohol/ketone ratios (A/K) between 6.7 and 12.3 were obtained, which is consistent with the involvement of a highly selective metal-centered oxidant as the active species in these reactions.[28] When the H_2O_2 concentration was increased up to 100 equiv, the efficiency of the oxidations slightly decreased, giving yields down to 26−60%, and the A/K ratio also decreased (Table 7). However, these catalysts are still among the most efficient for such transformation,[5b,29] and up to now, the catalytic results disclosed here have only been surpassed by two previously reported iron complexes under analogous conditions.[30]

Careful analysis of the catalytic results indicates that both the catalytic efficiency and the A/K ratio are essentially the same for all complexes belonging to class I ($^{H,R'}$**1**), meaning that the electronic properties of the γ-substituent in the pyridine ring do not significantly influence the catalytic activity. Instead, the introduction of a methyl substituent in the α-position of the pyridine (^{Me,H}**1** and ^{Me,Me}**1**) gives catalysts that afford minimal depletion of efficiency when the amount of oxidant is increased. This is exemplified for catalyst ^{Me,Me}**1**, which converts hydrogen peroxide into products in 60% yield with either 10 or 100 equiv of H_2O_2. Therefore, these catalysts appear to be good candidates to catalyze C−H hydroxylation under preparative scale conditions. As a matter of fact, some of us have recently demonstrated that ^{Me,H}**1** is a remarkably efficient and selective

dx.doi.org/10.1021/ic4004033 | Inorg. Chem. 2013, 52, 9229−9244

catalyst in alkane C−H hydroxylation under preparative conditions.[11b]

The oxidation of *cis*-cyclooctene with 10 equiv of H_2O_2 by complexes $^{R,R'}$**1** afforded high yields (between 72 and 95%) of products as a mixture of *syn*-diol (D)[27] and epoxide (E). Even when the amount of H_2O_2 was increased up to 100 equiv, the yields remained at the same level, with the single exception of ^{H,NO2}**1** that showed modest efficiency under these conditions. Such high efficiencies in the conversion of oxidant into oxidized products indicate that the complexes described in this work could be potentially suitable for alkene oxidation for synthetic purposes. The diol/epoxide ratio (D/E) was modest for most complexes (D/E = 1−2), except for ^{Me,H}**1**, ^{Cl,H}**1**, and ^{Me,Me}**1** belonging to class II, which exhibited D/E values up to 6.2. This observation suggests that these three complexes could be used as catalysts for the preparation of *syn*-diols.[31]

Isotopic Labeling Studies in the Oxidation of Cyclooctene. Isotopic labeling experiments were devised to investigate if this set of complexes operates through a common reaction mechanism. Two main mechanisms of action have been proposed for iron catalysts that mediate olefin *cis*-dihydroxylation with H_2O_2 (Scheme 2). On the one hand, some catalysts operate through an Fe^{III}/Fe^{V} catalytic cycle with $Fe^{V}(O)(OH)$ as the active species, which is formed via water-assisted O−O cleavage of $Fe^{III}(OOH)(OH_2)$.[23,32] Consequently, the oxygen inventory in $Fe^{V}(O)(OH)$ is composed of one oxygen atom that comes from the oxidant (H_2O_2), and the second one is derived from water. Rapid oxo−hydroxo tautomerism explains that oxygen atoms originally coming from water end up being incorporated as terminal oxo ligands. Initial electrophilic attack of the hydroxyl ligand of $Fe^{V}(O)(OH)$ toward an olefin results in a *cis*-dihydroxylation reaction[32b] so that the two oxygen atoms of the $Fe^{V}(O)(OH)$ species end up in the corresponding *syn*-diol product. C−H hydroxylation and olefin epoxidation by $Fe^{V}(O)(OH)$ are initiated by the oxo ligand and occur with stereoretention. On the other hand, other catalysts operate via an Fe^{II}/Fe^{IV} catalytic cycle where $Fe^{IV}(O)(OH_2)$ or $Fe^{IV}(OH)_2$ is the key oxidizing species.[33]

Scheme 2. Water-Assisted (Fe^{III}/Fe^{V}) and Non-Water-Assisted (Fe^{II}/Fe^{IV}) Mechanisms To Explain the Oxidation of Olefins by Mononuclear Non-Heme Iron Catalysts

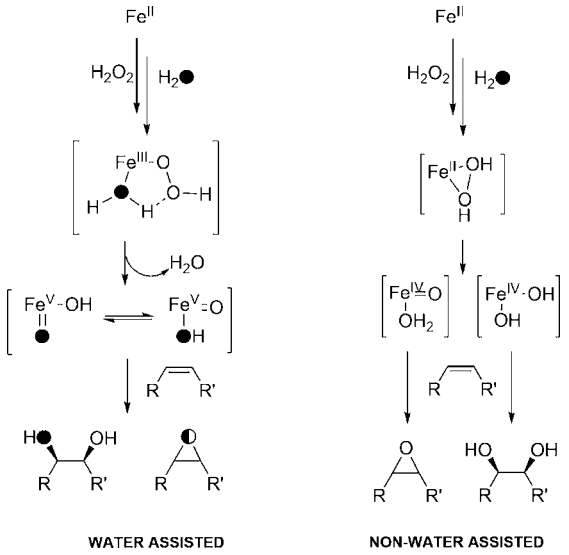

When this mechanism is operative, in contrast to the Fe^{III}/Fe^{V} pathway, the two oxygen atoms in the *syn*-diol originate from the oxidant. Therefore, the isotopic labeling pattern observed in the *cis*-dihydroxylation of olefins contains essential information about the nature of the oxidizing species.

Labeling experiments have been carried out by oxidizing *cis*-cyclooctene (100 equiv) in the presence of $H_2{}^{18}O$ (1000 equiv) using H_2O_2 as oxidant (10 equiv) (Table 7). For all catalysts, most of the *syn*-diol product contains one oxygen atom coming from water (89 ± 10% singly ^{18}O-labeled diol).[27] The other oxygen atom incorporated into the *syn*-diol product originates from H_2O_2, as previously reported for catalysts ^{H,H}**1** and ^{Me,H}**1** using $H_2{}^{18}O_2$ as oxidant.[11a,32d] Clear-cut differences between class I and class II complexes arise when the labeling results for the other product of the reaction, cyclooctene oxide, are analyzed. Incorporation of water into the epoxide product is very high for class I complexes (70 ± 7%), while for class II complexes the amount of ^{18}O-labeled epoxide dramatically decreases to 7 ± 3% (Table 7). A similar trend in the ^{18}O-content (i.e., high and low incorporation for class I and class II, respectively) has been previously observed in alcohol products obtained in the hydroxylation of alkanes in the presence of $H_2{}^{18}O$.[27] Therefore, by analyzing the isotope labeling in *cis*-dihydroxylation and the epoxidation products, we conclude that class I and class II catalysts operate via a water-assisted pathway with a common $Fe^{V}(O)(OH)$ oxidant. However, while the oxo ligand transferred to cyclooctene in class I catalysts mainly originates from water, it almost exclusively comes from H_2O_2 in class II, as ascertained from the labeling results in the epoxide product. Some involvement of the nonwater-assisted mechanism (Scheme 2, right) cannot be ruled out, particularly for class II complexes for which a lower percentage of ^{18}O-atom incorporation into the *cis*-diol is observed (78−89% for class II compared to 95−99% for class I).

It is also important to notice that within class I catalysts the percentage of water incorporation into the epoxide is slightly tuned by the electronic properties of the γ-substituent in the pyridine ring, though this effect is much subtler. Catalysts with no substituent (^{H,H}**1**) or an electron-rich group in the γ-position (^{H,Me}**1**, ^{H,NMe2}**1**, and ^{H,OMe}**1**) afford epoxide with an ^{18}O-content roughly 10% higher compared to catalysts with electron-withdrawing groups (^{H,Cl}**1**, ^{H,NO2}**1**, and ^{H,CO2Et}**1**) (74 ± 3 versus 65 ± 2%).

In a previous mechanistic study on the olefin epoxidation reaction catalyzed by ^{H,H}**1**, we concluded that because the two coordination sites where oxo and hydroxide ligand binding occur are not identical, the $Fe^{V}(O)(OH)$ species (**4**) can exist as two tautomers, which are related by a fast water-assisted equilibrium (Scheme 3).[32d] The difference between these two isomers is the relative position of the oxo and the hydroxide ligand. While in the isomer $Fe^{V}(O_A)(O_BH)$ (**4a**), the oxo ligand binds in position A, which is *trans* to the NCH_2Py unit, in isomer $Fe^{V}(O_B)(O_AH)$ (**4b**), the oxo group is located *trans* to one of the *N*-methyl groups (position B). As hydrogen peroxide binding in the preceding $Fe^{III}(OOH)(H_2O)$ intermediate (**3**) takes place preferentially in the B-position,[27] water binding occurs mainly in position A. Thus, the relative reactivity of **4a** and **4b** determines the percentage of oxygen from water that is incorporated into the oxidized product. In the particular case of ^{H,H}**1**, this value was found to be dependent on the nature of the olefin. *Cis*-olefins were epoxidized with ∼60−70% incorporation of water, while *trans*- and terminal olefins incorporated substantially smaller amounts of water (∼30%).[32d]

dx.doi.org/10.1021/ic4004033 | *Inorg. Chem.* 2013, 52, 9229−9244

Scheme 3. Proposed Mechanism for Alkene Oxidation, Where the Fast Equilibrium between the Two Tautomers 4a and 4b Is Represented

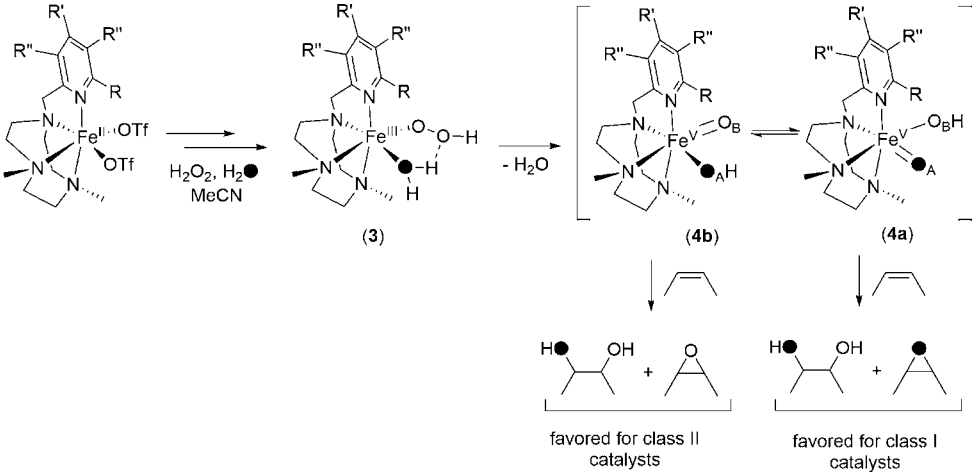

The present analysis indicates that the relative reactivity of the two tautomers is only slightly modified when the electronic properties of the pyridine are altered by introducing electron-releasing or electron-withdrawing groups at the γ-position. This conclusion is not surprising if it is taken into account that the pyridine ligand is disposed in a relative *cis*-position with respect to the two coordination sites occupied by the oxo and hydroxide ligands (Scheme 3). Ligands in relative *cis*-position are expected to have a smaller effect than those in *trans* because the latter facilitates electronic communication between the two ligands. Instead, the introduction of sterically more-demanding groups at the α-position of the pyridine has a profound impact on the relative reactivity of **4a**/**4b** and, in turn, in the epoxide labeling result. Indeed, a space-filling analysis (Figure 1) shows that position A, which falls in the same plane as the pyridine ring, is in close proximity to the α-pyridine substituent and presumably becomes less accessible to the substrate. As a consequence, isomer **4a** becomes less reactive, and the percentage of water incorporated into the products is diminished. With these premises, we suggest that steric interactions produce a more-sensitive modification of the relative reactivity of the two tautomers. However, further clarification of this point is under study.

CONCLUSIONS

In the present work, we have described the synthesis and the characterization of a broad family of mononuclear iron complexes containing a derivatized Pytacn ligand structure. We have demonstrated that the introduction of different substituents in the pyridine ring causes modest but systematic effects in the geometric parameters of the resulting complexes and substantial changes in the electronic properties of the iron center. Modification of the electronic properties of the iron center are achieved by introducing different substituents in the γ-position of the pyridine ring (class I complexes). These modifications become important to systematically and consistently define the spin state of the iron center in this class of complexes, for which the LS and HS configurations are energetically very close. In particular, for $^{H,R'}$**2**OTf complexes, the effect of the γ-substituent can be understood in accordance with simple ligand field theory; the LS contribution is more important upon increasing the π-acceptor character of the pyridine, which is modulated by the electron-releasing ability of the γ-substituent. On the other hand, the presence of substituents in the α-position of the pyridine (class II compounds) introduces steric constraints that cause dramatic modifications in the properties of the iron center by favoring the HS configuration over the LS configuration.

Although all complexes presented herein behave as highly efficient catalysts in the oxidation of C−H and C═C bonds using H_2O_2 as the oxidant through the intermediacy of a common $Fe^V(O)(OH)$ oxidant, there are some clear differences among them. The presence of a methyl group in the α-position of the pyridine ring affords catalysts that maintain their activity at higher oxidant concentrations and exhibit remarkably high D/E ratios in the oxidation of cyclooctene. Differences between class I and class II catalysts are evidenced in the ^{18}O-content of the epoxide product for experiments carried out in the presence of $H_2{}^{18}O$. Complexes without any substituent in the α-position (class I) exhibit much higher levels of oxygen incorporation from water into the oxidized products than those bearing a substituent in this position (class II). Although the effect of the introduction of a substituent in the α-position is important, the electronic properties of the group in the γ-position of the pyridine only induce minimal modifications. Thus, steric demands in close proximity to the iron site emerge from this study as key structural aspects defining not only the relative reactivity of the two tautomeric active $Fe^V(O)(OH)$ species but also the chemoselectivity toward *cis*-dihydroxylation over epoxidation.

EXPERIMENTAL SECTION

Materials. Reagents and solvents were of commercially available reagent quality unless otherwise stated. $H_2{}^{18}O$ (95% ^{18}O-enriched) was received from ICON Isotopes. Solvents were purchased from SDS and Scharlab.

Physical Measurements. IR spectra were taken in a Mattson-Galaxy Satellite FT-IR spectrophotometer using a MKII Golden Gate single reflection ATR system. UV−vis spectroscopy was performed on a Cary 50 Scan (Varian) UV−vis spectrophotometer with 1 cm quartz cells. NMR spectra were taken on a Bruker DPX200, 300 or 400 MHz spectrometer using standard conditions. Elemental analyses were performed using a CHNS-O EA-2400 serie II from Perkin-Elmer. The ESI-MS experiments were performed on a HPLC/MS chromatograph, HPLC from Agilent 1100 Series and MS from Bruker Daltonics, Esquire6000 Ion Trap or on a Bruker micrOTOF Q (II) spectrometer using acetonitrile as a mobile phase. Product analyses were performed

dx.doi.org/10.1021/ic4004033 | Inorg. Chem. 2013, 52, 9229−9244

on an Agilent 7820A gas chromatograph (HP5 column, 30m or Cyclosil-B column, 30m) and a flame ionization detector. GC-MS spectral analyses were performed on an Agilent 7890A gas chromatograph interfaced with an Agilent 5975c MS mass spectrometer. A 50% NH_3/CH_4 mix was used as the ionization gas for chemical ionization analyses. The products were identified by comparison of their GC retention times and GC/MS with those of authentic compounds. Variable-temperature magnetic susceptibility was obtained on microcrystalline samples with a Quantum Design MPMS-XL SQUID magnetometer. Solution magnetic susceptibility measurements were measured by NMR by the Evans' method[34] using special coaxial insert tubes purchased from Wilmad Glass, Co. Temperature-dependent density of the solvent acetonitrile has been taken into account for the measurement of the magnetic moments (Evans' method) and UV−vis spectra at variable temperature.

Crystal-Structure Determination. The measurements were carried out on a BRUKER SMART APEX CCD diffractometer using graphite-monochromated Mo Kα radiation (λ = 0.71073 Å) from an X-ray tube. Programs used: data collection, Smart version 5.631 (Bruker AXS 1997−02); data reduction, Saint + version 6.36A (Bruker AXS 2001); absorption correction, SADABS version 2.10 (Bruker AXS 2001). Structure solution and refinement were done using SHELXTL version 6.14 (Bruker AXS 2000−2003) and SHELXT version 2013_3. The structures were solved by direct methods and refined by full-matrix least-squares methods on F^2. The non-hydrogen atoms were refined anisotropically. The H atoms were placed in geometrically optimized positions and forced to ride on the atom to which they are attached. Although crystal data indicate that the X-ray structures of ^{H,NMe2}**1** and ^{F,H}**1** are not fully satisfactory, they are of sufficient quality for the discussion of the crystallographic parameters made in the present work.

Synthesis of Ligands. Syntheses and full characterization of ligands $^{R,R'}$Pytacn are included in the Supporting Information.

Synthesis of Complexes. *Synthesis of Bis-triflato Complexes [Fe(OTf)$_2$($^{R,R'}$Pytacn)] ($^{R,R'}$**1**).* $^{R,R'}$**1** complexes were prepared in a glovebox ([O_2] < 1 ppm, [H_2O] < 1 ppm). [Fe(OTf)$_2$(^{H,H}Pytacn)] (^{H,H}**1**)[12] and [Fe(OTf)$_2$(^{Me,H}Pytacn)] (^{Me,H}**1**)[11a] were synthesized as previously reported. Single crystals of compounds $^{R,R'}$**1** suitable for X-ray analyses were obtained by slow diethyl ether diffusion into CH_2Cl_2 solutions of the complexes.

*[Fe(OTf)$_2$(^{H,Me}Pytacn)] (^{H,Me}**1**).* A suspension of [Fe(OTf)$_2$(CH_3CN)$_2$] (176 mg, 0.40 mmol) in CH_2Cl_2 (2 mL) was added dropwise to a vigorously stirred solution of ^{H,Me}Pytacn (106 mg, 0.40 mmol) in CH_2Cl_2 (1 mL). The iron triflate salt quickly solubilized affording a dark red solution, which was stirred for 3 h. Afterward, the solution was filtered and slow diethyl ether diffusion afforded 190 mg of yellow crystals (0.31 mmol, 77%). Anal. Calcd for $C_{17}H_{26}F_6FeN_4O_6S_2$: C, 33.13; H, 4.25; N, 9.09. Found: C, 33.29; H, 4.07; N, 9.12. ^{1}H NMR (CD_3CN, 200 MHz, 300 K) δ, ppm: 14.66, 11.17, 7.73, 5.46. ^{1}H NMR (CD_2Cl_2, 200 MHz, 300 K) δ: 145.68, 119.76, 92.89, 48.61, 35.44, −11.56. ESI-MS (m/z): 159.1 [M − 2OTf]$^{2+}$.

*[Fe(OTf)$_2$(^{H,NMe2}Pytacn)] (^{H,NMe2}**1**).* Prepared in analogous manner to ^{H,Me}**1**. Yield = 69%. Anal. Calcd for $C_{18}H_{29}F_6FeN_5O_6S_2$: C, 33.50; H, 4.53; N, 10.85. Found: C, 33.67; H, 4.33; N, 10.82. FT-IR (ATR) ν, cm^{-1}: 2916−2872 (C−H)$_{sp3}$, 1298 (py), 1219, 1158, 1027, 1010, 632 (CF_3SO_3). ^{1}H NMR (CD_3CN, 400 MHz, 300 K) δ, ppm: 44.52, 34.32, 29.21, 20.73, 18.80, 12.11, 6.90. ^{1}H NMR (CD_2Cl_2, 400 MHz, 300 K) δ, ppm: 120.50, 108.63, 83.25, 42.69, 39.49. ESI-MS (m/z): 496.0 [M − OTf]$^+$ (100), 173.5 [M − 2OTf]$^{2+}$ (25).

*[Fe(OTf)$_2$(^{H,OMe}Pytacn)] (^{H,OMe}**1**).* Prepared in analogous manner to ^{H,Me}**1**. Yield = 38%. Anal. Calcd for $C_{19}H_{30}F_6FeN_4O_7S_2$: C, 34.55; H, 4.58; N, 8.48. Found: C, 34.59; H, 4.43; N, 8.64. FT-IR (ATR) ν, cm^{-1}: 2968−2888 (C−H)$_{sp3}$, 1468 (py), 1250, 1157, 1026, 635 (CF_3SO_3). ^{1}H NMR (CD_3CN, 400 MHz, 300 K) δ, ppm: 13.41, 11.60, 8.80, 6.49, 3.64. ^{1}H NMR (CD_2Cl_2, 400 MHz, 300 K) δ, ppm: 120.38, 114.44, 94.31. ESI-MS (m/z): 511.1 [M − OTf]$^+$ (25), 181.0 [M − 2OTf]$^{2+}$ (100).

*[Fe(OTf)$_2$(^{H,Cl}Pytacn)] (^{H,Cl}**1**).* A solution of [Fe(OTf)$_2$(CH_3CN)$_2$] (155 mg, 0.36 mmol) in anhydrous THF (2 mL) was added dropwise to a vigorously stirred solution of ^{H,Cl}Pytacn (101 mg, 0.36 mmol) in THF (1.5 mL). After a few seconds the solution became cloudy and a pale yellow precipitate appeared. After being stirred for 2 h the solution was filtered off and the resulting yellow solid dried under vacuum. This solid was dissolved in CH_2Cl_2 and filtered through Celite. Slow diethyl ether diffusion over the resulting solution afforded, in a few days, 143 mg of yellow crystals (0.22 mmol, 63%). Anal. Calcd for $C_{16}H_{23}ClF_6FeN_4O_6S_2$: C, 30.18; H, 3.64; N, 8.80; S, 10.07. Found: C, 30.09; H, 3.62; N, 8.88; S, 9.95. FT-IR (ATR) ν, cm^{-1}: 2960−2885 (C−H)$_{sp3}$, 1281 (py), 1222, 1161, 1027, 634 (CF_3SO_3). ^{1}H NMR (CD_3CN, 400 MHz, 300 K) δ, ppm: 12.44, 9.53, 7.07, 5.45, 3.95, 3.43, 2.18, 1.13. ^{1}H NMR (CD_2Cl_2, 400 MHz, 300 K) δ, ppm: 157.29, 119.78, 100.05, 89.73, 47.813, 33.75. ESI-MS (m/z): 487.0 [M − OTf]$^+$ (100), 168.9 [M − OTf]$^{2+}$ (25).

*[Fe(OTf)$_2$(^{H,CO2Et}Pytacn)] (^{H,CO2Et}**1**).* Prepared in analogous manner to ^{H,Cl}**1**. Yield = 43%. Anal. Calcd for $C_{19}H_{28}F_6FeN_4O_8S_2$: C, 33.84; H, 4.18; N, 8.31. Found: C, 33.48; H, 3.97; N, 8,63. FT-IR (ATR) ν, cm^{-1}: 2982−2865 (C−H)$_{sp3}$, 1732 (C═O), 1284 (py), 1284, 1224, 1164, 1026, 633 (CF_3SO_3). ^{1}H NMR (CD_3CN, 400 MHz, 300 K) δ, ppm: 10.84, 8.89, 5.76, 4.83, 4.36, 4.39, 3.04, 2.11, 1.97. ^{1}H NMR (CD_2Cl_2, 400 MHz, 300 K) δ, ppm: 164.22, 103.84, 90.26, 49.67, 39.01. ESI-MS (m/z): 525.1 [M − OTf]$^+$ (25), 188.0 [M − 2OTf]$^{2+}$ (100).

*[Fe(OTf)$_2$(^{H,NO2}Pytacn)] (^{H,NO2}**1**).* Prepared in analogous manner to ^{H,Me}**1**. Yield =73%. Anal. Calcd for $C_{16}H_{23}F_6FeN_5O_8S_2$: C, 29.69; H, 3.58; N, 10.82; S, 9.91. Found: C, 29.87; H, 3.70; N, 10.81; S, 9.76. FT-IR (ATR) ν, cm^{-1}: 2917 (C−H)$_{sp3}$, 1279 (py), 1223, 1159, 1028, 633 (CF_3SO_3). ^{1}H NMR (CD_3CN, 400 MHz, 300 K) δ, ppm: 10.47, 8.73, 4.93, 4.17, 7.78, 2.86, 2.64, 2.14, 1.13. ^{1}H NMR (CD_2Cl_2, 400 MHz, 300 K) δ, ppm: 174.18, 136.30, 108.77, 92.12, 47.82, 33.18. ESI-MS (m/z): 498.0 [M − OTf]$^+$ (100), 174.5 [M − 2OTf]$^{2+}$ (100).

*[Fe(OTf)$_2$(^{Me,Me}Pytacn)] (^{Me,Me}**1**).* Prepared in analogous manner to ^{H,Me}**1**. Yield = 59%. Anal. Calcd for $C_{18}H_{28}F_6FeN_4O_6S_2$: C, 34.30; H, 4.48; N, 8.89. Found: C, 34.37; H, 4.11; N, 8.83. ^{1}H NMR (CD_3CN, 200 MHz, 300 K) δ, ppm: 138.63, 84.64, 54.02, 47.91, 42.83, 31.14, 13.71, −32.78. ^{1}H NMR (CD_2Cl_2, 200 MHz, 300 K) δ, ppm: 176.16, 130.18, 101.05, 95.33, 60.52, 52.75, 38.97, −1.70, −37.25. ESI-MS (m/z): 166.1 [M − 2OTf]$^{2+}$, 481.12 [M − OTf]$^+$.

*[Fe(OTf)$_2$(^{Cl,H}Pytacn)] (^{Cl,H}**1**).* Prepared in analogous manner to ^{H,Cl}**1**. Yield = 66%. Anal. Calcd for $C_{16}H_{23}F_6ClFeN_4O_6S_2$: C, 30.18; H, 3.64; N, 8.80. Found: C, 29.98; H, 3.58; N, 8.68. FT-IR (ATR) ν, cm^{-1}: 3357−3262 (C−H)$_{sp3}$, 1281, 1226, 1163, 1027, 630 (CF_3SO_3). ^{1}H NMR (CD_3CN, 200 MHz, 300 K) δ, ppm: 100.19, 60.14, 39.41. ^{1}H NMR (CD_2Cl_2, 400 MHz, 300 K) δ, ppm: 155.97, 121.95, 106.25, 101.89, 89.16, 75.50, 60.30, 44.68, 32.45, 18.57. ESI-MS (m/z): 169.0 [M − 2OTf]$^{2+}$, 487.1 [M − OTf]$^+$.

*[Fe(OTf)$_2$(^{F,H}Pytacn)] (^{F,H}**1**).* Prepared in analogous manner to ^{H,Cl}**1**. Yield = 27%. Anal. Calcd for $C_{16}H_{23}F_7FeN_4O_6S_2$: C, 30.98; H, 3.74; N, 9.03. Found: C, 31.06; H, 3.43; N, 9.28. FT-IR (ATR) ν, cm^{-1}: 2927 (C−H)$_{sp3}$, 1309, 1213, 1158, 1015, 630 (CF_3SO_3). ^{1}H NMR (CD_3CN, 200 MHz, 300 K) δ, ppm: 104.67, 84.41, 70.10, 50.59, 28.53, −2.91 . ^{1}H NMR (CD_2Cl_2, 200 MHz, 300 K) δ, ppm: 142.65, 122.50, 108.05, 80.16, 69.76, 29.99, 18.95. ESI-MS (m/z): 161.0 [M − 2OTf]$^{2+}$, 471.1 [M − OTf]$^+$.

*[Fe(^{H,H}Pytacn)(CH_3CN)$_2$](SbF$_6$)$_2$ (^{H,H}**2**SbF$_6$).* $FeCl_2$ (51 mg, 0.40 mmol) was added directly as a solid to a vigorously stirred solution of ^{H,H}Pytacn (100 mg, 0.40 mmol) in CH_3CN. The initially pale yellow solution became gradually bright orange as the $FeCl_2$ got dissolved. After being stirred for 30 min, $AgSbF_6$ (277 mg, 0.80 mmol) was added which caused the immediate precipitation of AgCl and an evident color change of the solution from bright orange to dark brown. After being stirred for 30 min, the solution was filtered through Celite. Slow diethyl ether diffusion over the resulting solution afforded, in a few days, 245 mg of red-brown crystals (0.29 mmol, 71% yield). Anal. Calcd for $C_{18}H_{30}F_{12}FeN_6Sb_2$: C, 25.20; H, 3.53; N, 9.80. Found: C, 25.44; H, 3.47; N, 10.15. ^{1}H NMR (CD_3CN, 400 MHz, 300 K) δ, ppm: 12.68, 9.73, 9.59, 9.10, 7.33, 6.70, 3.82, 2.17, 1.96. HRMS (m/z): 152.0668 [M − 2CH_3CN−2SbF$_6$]$^{2+}$, 161.0718 [M − 2CH_3CN−2SbF$_6$ + H_2O]$^{2+}$, 539.0312 [M − 2CH_3CN−SbF$_6$]$^+$.

dx.doi.org/10.1021/ic4004033 | Inorg. Chem. 2013, 52, 9229−9244

*[Fe(^{Me,H}Pytacn)(CH$_3$CN)$_2$](SbF$_6$)$_2$ (^{Me,H}**2**SbF$_6$).* $FeCl_2$ (11 mg, 0.09 mmol) was added directly as a solid to a vigorously stirred solution of ^{Me,H}Pytacn (21 mg, 0.09 mmol) in CH_3CN. The initially pale yellow solution became gradually bright orange as the $FeCl_2$ got dissolved. After being stirred for 30 min, $AgSbF_6$ (60 mg, 0.17 mmol) was added which caused the immediate precipitation of AgCl and an evident color change of the solution from bright orange to yellowish. After being stirred for 30 min, the solution was filtered through Celite. Slow diethyl ether diffusion over the resulting solution afforded, in a few days, 54 mg of colorless crystals which were suitable for X-ray diffraction (0.05 mmol, 69% yield). Anal. Calcd for $C_{19}H_{32}F_{12}FeN_6Sb_2$: C, 26.18; H, 3.70; N, 9.64%. Found: C, 26.16; H, 3.45; N, 8.94% (repeated attempts to improve the accuracy of the elemental analysis were unsuccessful). ^{1}H NMR (CD_3CN, 400 MHz, 300 K) δ, ppm: 143.94, 84.76, 56.30, 49.10, −7.74, −32.53. ESI-MS (m/z): 159.0759 [M − 2CH_3CN−2SbF_6]$^{2+}$, 553.0462 [M − 2CH_3CN−SbF_6]$^+$.

Reaction Conditions for Catalysis. In a typical reaction, 0.36 mL of a 70 mM (25 μmol) or 700 mM (250 μmol) H_2O_2 solution (diluted from a 35% H_2O_2 aqueous solution) in CH_3CN was delivered by syringe pump over 30 min at 25 °C to a vigorously stirred CH_3CN solution (2.14 mL) containing the iron catalyst (2.5 μmols) and the substrate (2500 μmols). The final concentrations of reagents were 1 mM iron catalyst, 10 mM/100 mM H_2O_2, and 1 M substrate. After syringe pump addition, the resulting solution was stirred for another 10 min. For the oxidation of cyclohexane, biphenyl (internal standard) was added at this point and the iron complex was removed by passing the solution through a short path of basic alumina or silica followed by elution with 2 mL of AcOEt. Finally, the solution was subjected to GC analysis. The organic products were identified by comparison with authentic compounds.

For the oxidation of cyclooctene, the reaction was performed as described above but under a N_2 atmosphere. After the oxidant was added by syringe pump and the mixture was stirred for 10 min, 1 mL of acetic anhydride together with 0.1 mL of 1-methylimidazole was added to afford the esterification of the diol product. After being stirred for 15 min at room temperature, ice was added and the mixture was stirred for about 30 min. Biphenyl (internal standard) was added and the mixture was extracted with 2 mL of $CHCl_3$. The organic layer was washed with 2 mL H_2SO_4 1M, 2 mL sat. $NaHCO_3$ and 2 mL H_2O, dried with $MgSO_4$ and subjected to GC analysis. The organic products were identified by comparison with authentic compounds.

Isotopic Labeling Experiments Using $H_2{}^{18}O$. The experimental procedure was similar to the one described above for a typical oxidation reaction of cyclooctene. In these experiments, 0.36 mL of a 70 mM (25 μmols) H_2O_2 solution were delivered by syringe pump over a solution containing the catalyst (2.5 μmols), 50 μL of $H_2{}^{18}O$ (2500 μmols) and cyclooctene (250 μmols) under an inert atmosphere. The incorporation of ^{18}O into the epoxide and *syn*-diol products was measured by GC-MS analyses. Specific ions corresponding to the epoxide and *syn*-diol mass spectra were computer simulated. In order to account for the isotopic purity of $H_2{}^{18}O$ and its dilution because of the use of aqueous H_2O_2 solutions, corrected values were obtained by dividing the simulated percentage of ^{18}O-labeled epoxide and $^{16}O^{18}O$-labeled *syn*-diol by 0.94.

■ ASSOCIATED CONTENT

Supporting Information

Description of the synthesis of $^{R,R'}$Pytacn ligands, solid-state characterization of ^{H,OMe}**1**, ^{H,Me}**1**, ^{H,Cl}**1**, ^{H,CO2Et}**1**, and ^{Cl,H}**1**, SQUID measurement for ^{Me,H}**2**SbF$_6$, paramagnetic ^{1}H NMR spectra of $^{R,R'}$**1** and $^{R,R'}$**2**, and variable-temperature paramagnetic ^{1}H NMR of ^{Me,H}**1**. This material is available free of charge via the Internet at http://pubs.acs.org.

■ AUTHOR INFORMATION

Corresponding Author

* E-mail: miquel.costas@udg.edu (M.C.), anna.company@udg.edu (A.C.).

Notes

The authors declare no competing financial interest.

■ ACKNOWLEDGMENTS

Financial support for this work was provided by the Spanish Ministry of Science (Project CTQ2012−37420-C02-01/BQU and Consolider Ingenio Ingenio/CSD2010-00065 to M.C. and X.R. and project CTQ2012-32436 to T.P.) and the European Research Council (ERC-2009-StG-239910 to M.C.). M.C. and X.R. acknowledge Generalitat de Catalunya for ICREA-Academia Awards and 2009-SGR637. A.C. acknowledges the European Commission for a Career Integration Grant (FP7-PEOPLE-2011-CIG-303522). The Spanish Ministry of Science is acknowledged for a FPU PhD grant to I.P. and for a Ramón y Cajal contract to A.C. We thank Catexel for a generous gift of tritosyl-1,4,7-triazacyclononane. X.R. is grateful for financial support from INNPLANTA project IPN-2011-0059-PCT-4200 0-ACT1.

■ REFERENCES

(1) (a) Meunier, B. *Biomimetic Oxidations Catalyzed by Transitons Metal Complexes*; Imperial College Press: London, 2000. (b) Arakawa, H.; Aresta, M.; Armor, J. N.; Barteau, M. A.; Beckman, E. J.; Bell, A. T.; Bercaw, J. E.; Creutz, C.; Dinjus, E.; Dixon, D. A.; Domen, K.; DuBois, D. L.; Eckert, J.; Fujita, E.; Gibson, D. H.; Goddard, W. A.; Goodman, D. W.; Keller, J.; Kubas, G. J.; Kung, H. H.; Lyons, J. E.; Manzer, L. E.; Marks, T. J.; Morokuma, K.; Nicholas, K. M.; Periana, R.; Que, L.; Rostrup-Nielson, J.; Sachtler, W. M. H.; Schmidt, L. D.; Sen, A.; Somorjai, G. A.; Stair, P. C.; Stults, B. R.; Tumas, W. *Chem. Rev.* **2001**, *101*, 953. (c) Bäckvall, J.-E. *Modern Oxidation Methods*; Wiley-VCH: Weinheim, Germany, 2004. (d) Shul'pin, G. B. *Mini-Rev. Org. Chem.* **2009**, *6*, 95.

(2) (a) Enthaler, S.; Junge, K.; Beller, M. *Angew. Chem., Int. Ed.* **2008**, *47*, 3317. (b) Schroder, K.; Junge, K.; Bitterlich, B.; Beller, M. In *Iron Catalysis: Fundamentals and Applications*; Plietker, B., Ed.; Springer-Verlag: Berlin, 2011; Vol. 33, p 83. (c) Mayer, A. C.; Bolm, C. Iron-Catalyzed Oxidation Reaction. In *Iron Catalyisis in Organic Chemistry*; Plietker, B., Ed.; Wiley-VCH: Weinheim, Germany, 2008; p 73. (d) Liang-Xian, L. *Curr. Org. Chem.* **2010**, *14*, 1099.

(3) (a) Ortiz de Montellano, P. R. *Chem. Rev.* **2010**, *110*, 932. (b) Ortiz de Montellano, P. R.; De Voss, J. J. *Nat. Prod. Rep.* **2002**, *19*, 477.

(4) (a) Tshuva, E. Y.; Lippard, S. J. *Chem. Rev.* **2004**, *104*, 987. (b) Bruijnincx, P. C. A.; van Koten, G.; Gebbink, R. *Chem. Soc. Rev.* **2008**, *37*, 2716. (c) Kovaleva, E. G.; Lipscomb, J. D. *Nat. Chem. Biol.* **2008**, *4*, 186. (d) Sazinsky, M. H.; Lippard, S. J. *Acc. Chem. Res.* **2006**, *39*, 558. (e) Costas, M.; Mehn, M. P.; Jensen, M. P.; Que, L. *Chem. Rev.* **2004**, *104*, 939.

(5) (a) Que, L., Jr.; Tolman, W. B. *Nature* **2008**, *455*, 333. (b) Talsi, E. P.; Bryliakov, K. P. *Coord. Chem. Rev.* **2012**, *256*, 1418. (c) Lu, H.; Zhang, P. *Chem. Soc. Rev.* **2011**, *40*, 1899. (d) Che, C. M.; Huang, J. S. *Chem. Commun.* **2009**, 3996. (e) Costas, M. *Coord. Chem. Rev.* **2011**, *255*, 2912.

(6) (a) Gibson, D. T.; Subramanian, V. In *Microbial Degradation of Aromatic Hydrocarbons*; Gibson, D. T., Ed.; Marcel Dekker: New York, 1984; p 181. (b) Gibson, D. T.; Parales, R. E. *Curr. Opin. Biotechnol.* **2000**, *11*, 236. (c) Chakrabarty, S.; Austin, R. N.; Deng, D. Y.; Groves, J. T.; Lipscomb, J. D. *J. Am. Chem. Soc.* **2007**, *129*, 3514.

(7) (a) Thibon, A.; Jollet, V.; Ribal, C.; Senechal-David, K.; Billon, L.; Sorokin, A. B.; Banse, F. *Chem.—Eur. J.* **2012**, *18*, 2715. (b) Moller, K.; Wienhofer, G.; Schroder, K.; Join, B.; Junge, K.; Beller, M. *Chem.—Eur. J.* **2010**, *16*, 10300.

(8) (a) Wang, B.; Wang, S. F.; Xia, C. G.; Sun, W. *Chem.—Eur. J.* **2012**, *18*, 7332. (b) Mikhalyova, E. A.; Makhlynets, O. V.; Palluccio, T. D.; Filatov, A. S.; Rybak-Akimova, E. V. *Chem. Commun.* **2012**, *48*, 687. (c) Oddon, F.; Girgenti, E.; Lebrun, C.; Marchi-Delapierre, C.; Pecaut, J.; Menage, S. *Eur. J. Inorg. Chem.* **2012**, 85. (d) Feng, Y.; England, J.; Que, L. *ACS Catal.* **2011**, *1*, 1035. (e) Wu, M.; Miao, C. X.; Wang, S. F.; Hu, X. X.; Xia, C. G.; Kuhn, F. E.; Sun, W. *Adv. Synth. Catal.* **2011**, *353*, 3014. (f) Bruijnincx, P. C. A.; Buurmans, I. L. C.; Gosiewska, S.; Moelands, M. A. H.; Lutz, M.; Spek, A. L.; van Koten, G.; Gebbink, R. *Chem.—Eur. J.* **2008**, *14*, 1228. (g) Liu, P.; Wong, E. L. M.; Yuen, A. W. H.; Che, C. M. *Org. Lett.* **2008**, *10*, 3275. (h) Comba, P.; Rajaraman, G. *Inorg. Chem.* **2008**, *47*, 78. (i) Mas-Balleste, R.; Que, L. *J. Am. Chem. Soc.* **2007**, *129*, 15964. (j) Marchi-Delapierre, C.; Jorge-Robin, A.; Thibon, A.; Ménage, S. *Chem. Commun.* **2007**, 1166. (k) Taktak, S.; Ye, W. H.; Herrera, A. M.; Rybak-Akimova, E. V. *Inorg. Chem.* **2007**, *46*, 2929. (l) Bukowski, M. R.; Comba, P.; Lienke, A.; Limberg, C.; de Laorden, C. L.; Mas-Balleste, R.; Merz, M.; Que, L. *Angew. Chem., Int. Ed.* **2006**, *45*, 3446. (m) Klopstra, M.; Roelfes, G.; Hage, R.; Kellogg, R. M.; Feringa, B. L. *Eur. J. Inorg. Chem.* **2004**, 846. (n) Dubois, G.; Murphy, A.; Stack, T. D. P. *Org. Lett.* **2003**, *5*, 2469. (o) Fujita, M.; Costas, M.; Que, L. *J. Am. Chem. Soc.* **2003**, *125*, 9912. (p) Ryu, J. Y.; Kim, J.; Costas, M.; Chen, K.; Nam, W.; Que, L. *Chem. Commun.* **2002**, 1288. (q) Mekmouche, Y.; Menage, S.; Toia-Duboc, C.; Fontecave, M.; Galey, J. B.; Lebrun, C.; Pecaut, J. *Angew. Chem., Int. Ed.* **2001**, *40*, 949. (r) White, M. C.; Doyle, A. G.; Jacobsen, E. N. *J. Am. Chem. Soc.* **2001**, *123*, 7194.

(9) (a) Roelfes, G.; Lubben, M.; Hage, R.; Que, L.; Feringa, B. L. *Chem.—Eur. J.* **2000**, *6*, 2152. (b) van den Berg, T. A.; de Boer, J. W.; Browne, W. R.; Roelfes, G.; Feringa, B. L. *Chem. Commun.* **2004**, 2550. (c) Romakh, V. B.; Therrien, B.; Suss-Fink, G.; Shul'pin, G. B. *Inorg. Chem.* **2007**, *46*, 3166. (d) Comba, P.; Maurer, M.; Vadivelu, P. *Inorg. Chem.* **2009**, *48*, 10389. (e) Mayilmurugan, R.; Stoeckli-Evans, H.; Suresh, E.; Palaniandavar, M. *Dalton Trans.* **2009**, 5101. (f) Gomez, L.; Garcia-Bosch, I.; Company, A.; Benet-Buchholz, J.; Polo, A.; Sala, X.; Ribas, X.; Costas, M. *Angew. Chem., Int. Ed.* **2009**, *48*, 5720. (g) Chen, M. S.; White, M. C. *Science* **2010**, *327*, 566. (h) Bruijnincx, P. C. A.; Buurmans, I. L. C.; Huang, Y. X.; Juhasz, G.; Viciano-Chumillas, M.; Quesada, M.; Reedijk, J.; Lutz, M.; Spek, A. L.; Munck, E.; Bominaar, E. L.; Gebbink, R. *Inorg. Chem.* **2011**, *50*, 9243. (i) Liu, P.; Liu, Y. G.; Wong, E. L. M.; Xiang, S.; Che, C. M. *Chem. Sci* **2011**, *2*, 2187. (j) Bigi, M. A.; Reed, S. A.; White, M. C. *Nat. Chem* **2011**, *3*, 216. (k) He, Y.; Gorden, J. D.; Goldsmith, C. R. *Inorg. Chem.* **2011**, *50*, 12651. (l) White, M. C. *Science* **2012**, *335*, 807. (m) Djernes, K. E.; Moshe, O.; Mettry, M.; Richards, D. D.; Hooley, R. J. *Org. Lett.* **2012**, *14*, 788. (n) Hitomi, Y.; Arakawa, K.; Funabiki, T.; Kodera, M. *Angew. Chem., Int. Ed.* **2012**, *51*, 3448. (o) Djernes, K. E.; Padilla, M.; Mettry, M.; Young, M. C.; Hooley, R. J. *Chem. Commun.* **2012**, *48*, 11576.

(10) (a) England, J.; Britovsek, G. J. P.; Rabadia, N.; White, A. J. P. *Inorg. Chem.* **2007**, *46*, 3752. (b) Mas-Ballesté, R.; Costas, M.; Berg, T. V. D.; Que, L., Jr. *Chem.—Eur. J.* **2006**, *12*, 7489. (c) Costas, M.; Que, L., Jr. *Angew. Chem., Int. Ed.* **2002**, *12*, 2179. (d) Chen, K.; Costas, M.; Que, L., Jr. *J. Chem. Soc., Dalton Trans.* **2002**, 672.

(11) (a) Company, A.; Gómez, L.; Fontrodona, X.; Ribas, X.; Costas, M. *Chem.—Eur. J.* **2008**, *14*, 5727. (b) Prat, I.; Gomez, L.; Canta, M.; Ribas, X.; Costas, M. *Chem.—Eur. J.* **2013**, *19*, 1908. (c) Garcia-Bosch, I.; Codola, Z.; Prat, I.; Ribas, X.; Lloret-Fillol, J.; Costas, M. *Chem.—Eur. J.* **2012**, *18*, 13269.

(12) Company, A.; Gómez, L.; Güell, M.; Ribas, X.; Luis, J. M.; Que, L., Jr.; Costas, M. *J. Am. Chem. Soc.* **2007**, *129*, 15766.

(13) Lloret, J.; Codolà, Z.; Garcia-Boch, I.; Gómez, L.; Pla, J. J.; Costas, M. *Nat. Chem.* **2011**, *3*, 807.

(14) (a) Garcia-Bosch, I.; Company, A.; Fontrodona, X.; Ribas, X.; Costas, M. *Org. Lett.* **2008**, *10*, 2095. (b) Garcia-Bosch, I.; Ribas, X.; Costas, M. *Adv. Synth. Catal.* **2009**, *351*, 348.

(15) (a) Diebold, A.; Hagen, K. S. *Inorg. Chem.* **1998**, *37*, 215. (b) Blakesley, D. W.; Payne, S. C.; Hagen, K. S. *Inorg. Chem.* **2000**, *39*, 1979. (c) Chen, K.; Que, L., Jr. *J. Am. Chem. Soc.* **2001**, *123*, 6327. (d) Britovsek, G. J. P.; England, J.; White, A. J. P. *Inorg. Chem.* **2005**, *44*, 8125. (e) Simaan, A. J.; Dopner, S.; Banse, F.; Bourcier, S.; Bouchoux, G.; Boussac, A.; Hildebrandt, P.; Girerd, J. J. *Eur. J. Inorg. Chem.* **2000**, 1627.

(16) (a) Zang, Y.; Kim, J.; Dong, Y.; Wilkinson, E. C.; Appelman, E. H.; Que, L., Jr. *J. Am. Chem. Soc.* **1997**, *119*, 4197. (b) Constable, E. C.; Baum, G.; Bill, E.; Dyson, R.; van Eldik, R.; Fenske, D.; Kaderli, S.; Morris, D.; Neubrand, A.; Neuburger, M.; Smith, D. R.; Wieghardt, K.; Zehnder, M.; Zuberbuhler, A. D. *Chem.—Eur. J.* **1999**, *5*, 498.

(17) Simaan, A. J.; Döpner, S.; Banse, F.; Bourcier, S.; Bouchoux, G.; Boussac, A.; Hildebrandt, P.; Girerd, J.-J. *Eur. J. Inorg. Chem.* **2000**, 1627.

(18) Marchivie, M.; Guionneau, P.; Létard, J. F.; Chasseau, D. *Acta Crystallogr., Sect. B: Struct. Sci.* **2003**, 479.

(19) Mashuta, M. S.; Webb, R. J.; McCusker, J. K.; Schmitt, E. A.; Oberhausen, K. J.; Richardson, J. F.; Buchanan, R. M.; Hendrickson, D. N. *J. Am. Chem. Soc.* **1992**, *114*, 3815.

(20) Ming, L.-J. In *Physical Methods in Bioinorganic Chemistry*; Que, L., Jr., Ed.; University Science Books: Sausalito, CA, 2000; p 375.

(21) (a) England, J.; Gondhia, R.; Bigorra-Lopez, L.; Petersen, A. R.; White, A. J. P.; Britovsek, G. J. P. *Dalton Trans.* **2009**, 5319. (b) England, J.; Davies, C. R.; Banaru, M.; White, A. J. P.; Britovsek, G. J. P. *Adv. Synth. Catal.* **2008**, *350*, 883. (c) Benhamou, L.; Thibon, A.; Brelot, L.; Lachkar, M.; Mandon, D. *Dalton Trans.* **2012**, *41*, 14369.

(22) Bryliakov, K. P.; Duban, E. A.; Talsi, E. P. *Eur. J. Inorg. Chem.* **2005**, *1*, 72.

(23) Chen, K.; Costas, M.; Kim, J.; Tipton, A. K.; Que, L., Jr. *J. Am. Chem. Soc.* **2002**, *124*, 3026.

(24) Machkour, A.; Mandon, D.; Lachkar, M.; Welter, R. *Inorg. Chem.* **2004**, *43*, 1545.

(25) (a) Balland, V.; Banse, F.; Anxolabéhère-Mallart, E.; Nierlich, M.; Girerd, J.-J. *Eur. J. Inorg. Chem.* **2003**, 2529. (b) Toftlund, H. *Coord. Chem. Rev.* **1989**, *94*, 67. (c) Bernal, I.; Jensen, I. M.; Jensen, K. B.; McKenzie, C. J.; Toftlund, H.; Tuchagues, J.-P. *J. Chem. Soc., Dalton Trans.* **1995**, 3667.

(26) (a) Mialana, P.; Nivorojkine, A.; Pratviel, G.; Azéma, L.; Slany, M.; Godde, F.; Simaan, A.; Banse, F.; Kargar-Grisel, T.; Bouchoux, G.; Sainton, J.; Horner, O.; Guilhem, J.; Tchertanova, L.; Meunier, B.; Girerd, J.-J. *Inorg. Chem.* **1999**, *38*, 1085. (b) Börzel, H.; Comba, P.; Hagen, K. S.; Lampeka, Y. D.; Lienke, A.; Linti, G.; Merz, M.; Pritzkow, H.; Tsymbal, L. V. *Inorg. Chim. Acta* **2002**, *337*, 407.

(27) Prat, I.; Company, A.; Postils, V.; Ribas, X.; Que, L., Jr.; Luis, J. M.; Costas, M. *Chem.—Eur. J.* **2013**, *19*, 6724.

(28) Costas, M.; Chen, K.; Que, L., Jr. *Coord. Chem. Rev.* **2000**, *200–202*, 517.

(29) Company, A.; Gomez, L.; Costas, M. In *Iron-Containing Enzymes: Versatile Catalysts of Hydroxylation Reactions in Nature*; De Visser, S. P., Kumar, D., Eds.; RSC: Cambridge, UK, 2011.

(30) (a) Chen, M. S.; White, M. C. *Science* **2007**, *318*, 783. (b) Gomez, L.; Canta, M.; Font, D.; Prat, I.; Ribas, X.; Costas, M. *J. Org. Chem.* **2013**, *78*, 1421.

(31) (a) Bataille, C. J. R.; Donohoe, T. J. *Chem. Soc. Rev.* **2011**, *40*, 114. (b) Chow, T. W.-S.; Wong, E. L.-M.; Guo, Z.; Liu, Y.; Huang, J.-S.; Che, C.-M. *J. Am. Chem. Soc.* **2010**, *132*, 13229. (c) Prat, I.; Font, D.; Company, A.; Junge, K.; Ribas, X.; Beller, M.; Costas, M. *Adv. Synth. Catal.* **2013**, *355*, 947.

(32) (a) Quinonero, D.; Morokuma, K.; Musaev, D. G.; Mas-Balleste, R.; Que, L., Jr. *J. Am. Chem. Soc.* **2005**, *127*, 6548. (b) Bassan, A.; Blomberg, M. R. A.; Siegbahn, P. E. M.; Que, L., Jr. *Angew. Chem., Int. Ed.* **2005**, *44*, 2939. (c) Prat, I.; Mathieson, J. S.; Ribas, X.; Güell, M.; Luis, J. M.; Cronin, L.; Costas, M. *Nat. Chem.* **2011**, *3*, 788. (d) Company, A.; Feng, Y.; Güell, M.; Ribas, X.; Luis, J. M.; Que, L., Jr.; Costas, M. *Chem.—Eur. J.* **2009**, *15*, 3359.

(33) (a) Bautz, J.; Comba, P.; Laorden, C. L. D.; Menzel, M.; Rajaraman, G. *Angew. Chem., Int. Ed.* **2007**, *46*, 8067. (b) Oldenburg, P. D.; Feng, Y.; Pryjomska-Ray, I.; Ness, D.; Que, L., Jr. *J. Am. Chem. Soc.* **2010**, *132*, 17713.

(34) (a) Naklicki, M. L.; White, C. A.; Plante, L. L.; Evans, C. E. B.; Crutchley, R. J. *Inorg. Chem.* **1998**, *37*, 1880. (b) Evans, D. F. *J. Chem. Soc.* **1959**, 2003.